MICROSPHERES IN THE VICINITY OF A BIFURCATION AT MODERATE REYNOLDS NUMBERS

Tristan Siou

Bachelor of Engineering
Mechatronic Engineering Major

Department of Electronic Engineering
Macquarie University

June 2017

Supervisor: Dr David Inglis

ACKNOWLEDGMENTS

I would like to acknowledge Dr David Inglis for the time he has taken to provide guidance and assistance every week, whether it be for making devices, laboratory work or writing. I would also like to thank Shilun and Lianmei for help around the laboratory and letting me use the microscope when I really needed to.

STATEMENT OF CANDIDATE

I, Tristan Siou, declare that this report, submitted as part of the requirement for the award of Bachelor of Engineering in the Department of Mechatronic Engineering, Macquarie University, is entirely my own work unless otherwise referenced or acknowledged. This document has not been submitted for qualification or assessment an any academic institution.

Student's Name: Tristan Siou

Student's Signature: T. Siou

Date: 6/11/17

ABSTRACT

In microfluidic filtration processes a mixture of particles in a suspension are separated by applying external forces on microparticles to displace particles of different characteristics. Microfluidic continuous flow filtration methods are passive filtration methods that separate particles by using a boundary that cause the particles to cross streamlines to be collected at different outputs. These methods can offer some advantages over other filtration methods as they require a relatively small sample sizes and they prevent clogging making the process efficient and cost effective. The devices used in this practice do not require a filter membrane which obstructs the particle path and often needs to be replaced, this means a range of particle sizes can be filtered using this method as long as they are small enough to pass through the channel of a device. One particular approach to microfluidic continuous flow filtration is uses channels with bifurcating channels of different flow rates to move particles of different sizes along different streamlines. This paper describes the motion of particles at the flow boundaries of these bifurcations at low to moderate Reynolds numbers to see if the fate of the particles near this boundary are affected by Reynolds number. This will be studied by running a stream of different sized polymer beads near a bifurcation and making observations of the particle path at different flow rates.

Contents

List of Figures

List of Tables

Chapter 1

Introduction

1.1 Lab-on-Chip Systems

Microfluidics is an exciting field that is now proving to be useful in many fields as technologies in the field can be used to assist in the separation and isolation of cells and particles for analysis and production. In the area of microfluidics the conduits for the separation of suspensions are diagnostic devices often referred to as micro-total-analyis systems μTAS or lab-on-chip (LOC) devices and are the technological focus of this field. LOC systems are designed in a way as to reduce macro-scale laboratory setups to a micro-scale setup that can fit on silicon or polymer chips akin to the development of integrated circuits and micro-electro-mechanical systems (MEMS). Reducing the scale of fluidic practices that deal with micron scale particle solutions is highly rewarding offering many advantages. A dramatic reduction of sample size is the main advantage of these devices allowing for fast analysis, efficient detection schemes and analysis for small volumes of fluid. These devices can be made portable and compact making them easier to use. These devices if viable will also be relatively cheap due to the small cost of materials needed and if mass produced their fabrication should also be relatively inexpensive.

1.2 Microfluidic Devices in Industry

LOC devices have been a useful tool in the research field in discovering uses for microfluidics in industry over the past with increasing publications in the various field every year but especially in the biomedical field. This research however has not translated over to the usage and creation of commercial products in these industries especially for clinical use and point of care (POC) products that can utilise LOC devices as they were originally

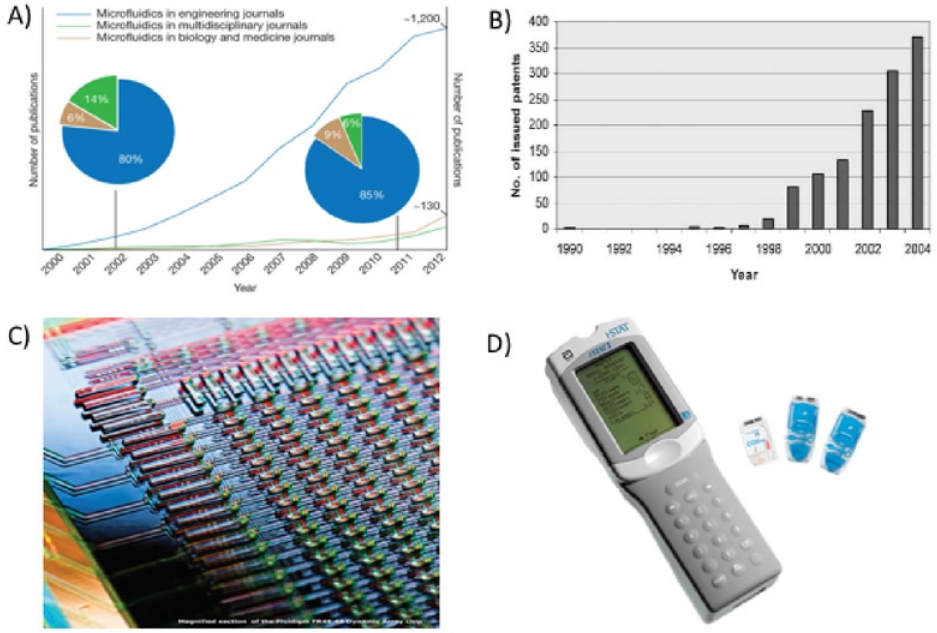

Figure 1.1: A) Information on the increasing number of publications in microfluidics. [6] B) A graph of the number of microfluidic device patents from 1990 to 2004 in the US. [2] C) Magnified section of a Fluidigm Dynamic Array Chip. [26] D) The i-STAT handheld POC device and the blood sample cartridges. [27]

designed for with the number of products with a low amount of products being released each year [1]. This is usually due to the high initial investment and running fabrication costs of production of the chips and is why many LOC device designs are often patented but not in use [9].

The cases where companies have released commercialised LOC microfluidic technologies in the biomedical field in areas such as gene sequencing and POC diagnostics [3]. Fluidigm Corporation is one of the companies in the field of genotyping that has managed to place marketable products for industry usage into production. There products focus on the use of integrated microfluidic circuits to sequence DNA samples to find particular gene structures [26]. These product have been used widely in finding epigenetic conditions, genetic mutations and diseases in various research and in clinical processes [7] [8]. These types of products need to be used by trained professionals and are mainly for

research purposes. The secondary area for the use of biomedical LOC systems, POC devices, focus on consumer level products that consumers can buy first hand from pharmaceutical companies to analyse biological sample. The company Abbott Laboratories has made available a hand held, POC device called the i-STAT which takes a blood sample cartridge and uses electrochemical detection to analyse blood chemistry. From these samples the device can quantify analytes such as electrolytes, metabolites, gases and some immunoassays [27]. POC technologies such as these are needed worldwide and as such current industry research into LOC devices are focused on the sample preparation and detection of biomarkers, biomolecular indicators of medical conditions for early diagnosis that commercialdevices such as the i-STAT cannot.

Unfortunately in the biomedical area the research, techniques for blood and cell separation such as continuous flow filtration has not translated well into commercial products due to current technology infrastructure even though the industry heavily requires pre-concentrated cell samples in processes such as the biomedical analysis in current industry research [4]. The continued research into this field and the LOC devices for it can hopefully act to improve these filtration so that they can overcome the issues of commercialisation.

1.3 Continuous Flow Filtration

There are various techniques that can be utilised in separation processes used in LOC systems. These techniques require the use of forces that can displace different particles based on characteristic properties such as density, charge, shape and size [11]. Laboratory technologies often require a large sample size at finite volumes to provide these forces and in cases like centrifugation the more delicate particles in biological samples are damaged in the process making the products redundant. For this reason LOC devices are designed as an alternative because it allows for continuous flow of particles leading to advantages such as a high throughput, visual feedback and lateral separation whilst keeping the sample size low [5]. These flows can be further combined with external fields in LOC devices to separate particles through magnetic or electric forces. For these reasons continuous flow filtration has been a technique popularly used in the research for blood sample separation. Here the use of various channel geometries have been explored to displace blood cells along different streamlines for high throughput separation however this has been proven difficult due to the deformable properties of red blood cell [11].

1.4 Hydrodynamic Filtration without Pores

The research detailed in this work looks at particles of different sizes around the separatrix where the flow behaviour separates at a T-shaped bifurcation seen in diagram in Fig.1.2. The separatrix is the line where the streamlines diverge causing the particles to move in along one of the two channels usually dependant on the particles size. These streamlines and the separatrix change with the velocity of the flow and if the flow is turbulent or laminar, which can be found using Reynolds number, Re. [11]

The reason for studying particles at the separatrix of T-shaped bifurcations is due to the large dynamic range of particles sizes possible. Any particles smaller than the channel can be separated using channels that have branching flows, this is possible by increasing the length of the perpendicular channel to increase its hydraulic resistance theoretically only allowing smaller particles through. Varying the size of the channel to allow larger particles to be separated from smaller particles is another reason branch flow filtration can allow for a large dynamic range. [16]

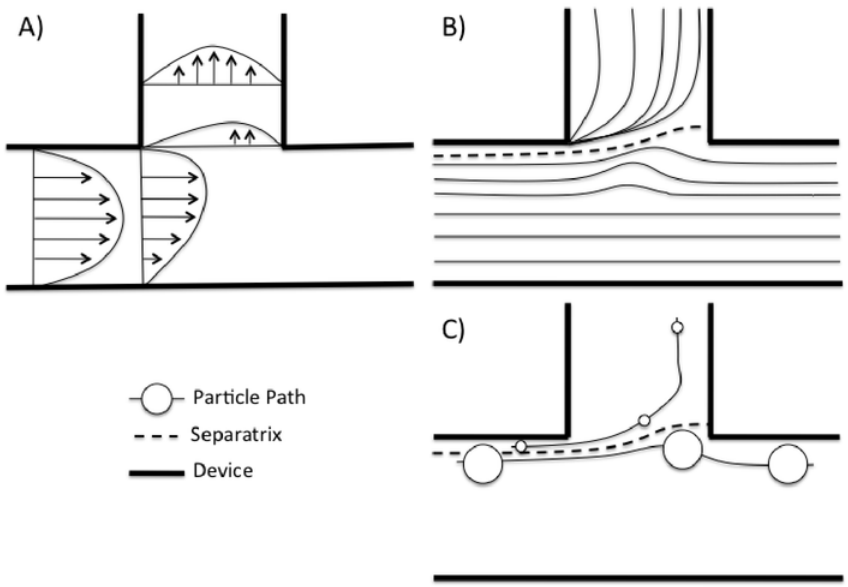

Figure 1.2: A) Diagram of the particle paths taken by different sized particles near the separatrix of a T-shaped bifurcation. B) The velocity profiles at along the main and perpendicular channel of the bifurcation. C) A representation of the streamlines occurring across the channels and how they change at the separatrix.

At these channel bifurcations the fraction of particles that travel down the channel with the higher flow rate is normally larger than the secondary branch, this is usually referred to as the Zweifach-Fung effect [15]. In many of the previous studies of microfluidic continuous filtration techniques the flow rates used are low, usually at $\mathrm{Re} \ll 1$, which cause the movement of particles to be more dependant on the viscous drag forces on the particles leading to the fate of the particles to be determined mostly by that effect however flows with speeds this low would not be used for real applications.

The final results of this paper should show how moderate Reynolds numbers will affect the separation of rigid particles when under soft inertial forces. The fate of particles near the separatrix should change independent of the flow rate ratios between the two channels due to variable inertial forces.

Chapter 2

Background and Theory

2.1 Introduction

This section will cover previous literature on microfluidic systems that look at branching as a method of filtration for particles. Many of these studies concern lab on chip devices, used for the filtration of either particles by size or the filtering of particles from a liquid.

2.2 Microfluidics Theory

2.2.1 Scaling Laws

Microfluidic systems behave differently to macroscopic systems due to scaling laws that change the importance of particular quantities that are determined a length, l. An example of the kinds of forces affected by these scaling laws are surface forces, l^2 such as surface tension gradients and shear stresses and volume forces, l^3, such as inertia and gravity. When these two types of forces are scaled down for use in microfluidics, surface forces become more dominant. This can be seen when you see the ratio for the two quantities as length decreases and the surface forces become proportionally much more significant [10].

$$\frac{l^2}{l^3} = \frac{1}{l} \tag{2.1}$$

As the volume forces decreases the surface forces quickly become much larger rendering the volume forces redundant.

2.2.2 Stokes Flow and Reynolds Number

In microfluidic devices the most important part of understanding these systems is to identify the properties of a fluid and how it influences its motion. The most common way that this motion can be defined is by using the Navier-Stokes equation. The Navier-Stokes equation describes the velocity, v, and pressure, p of a Newtonian fluid with density p and dynamic viscosity n across a channel [11].

$$p(dv/dt + (v.\nabla)v) = -\nabla\rho + n\nabla^2 v + f \tag{2.2}$$

F is used to represent body forces such as gravity, which becomes unimportant for micron scale devices, or external forces such as electrical forces.

Scaling laws are a major factor in causing the motion of fluids in microfluidic devices to act differently to macroscopic systems and as such the Navier-Stokes equation changes with it. The Navier-Stokes equation, due the characteristic channel dimension and low velocities of magnitudes between 10^{-3} to 10^{-6} of microfluidic systems cause the viscosity properties of the fluid become the major components of the equation. At the limiting velocities of microfluidic flows the complex inertial term $\rho(v.\nabla)v$ that defines the vector velocities across the flows cross section can be neglected making it easier to calculate the pressure and velocity of micro-channels, these flows are referred to as Stokes flow. To analyze Stokes flow the Navier-Stokes equation can be made dimensionless by expressing the equation as a ration of the inertial and viscous forces. The ratios between these forces give the dimensionless value Reynolds number, Re [10].

$$F_{inertial} = \frac{\rho V^2}{L} \tag{2.3}$$

$$F_{viscous} = \frac{\mu V}{L^2} \tag{2.4}$$

$$\frac{F_{inertial}}{F_{viscous}} = \frac{\rho V L}{\mu} = Re \tag{2.5}$$

In these equations, V is the characteristic fluid speed, L, the characteristic length of the channel, ρ is the density of the fluid and μ is viscosity.

When considering Re $\ll$ 1 the viscous term dominates and due to the inertia term being neglected this makes analysing stokes flow easier. Conversely when Re $>>$ 1 the inertial term dominates making it harder to analyse as the vector velocities of the flow

should be determined using differential equations to define the flows velocity fields [11]. For this reason a lot of the current literature in microfluidics avoid looking at higher Reynolds number analysis for the use in LOC devices.

2.3 Channel Behaviour

2.3.1 Poiseuille flow

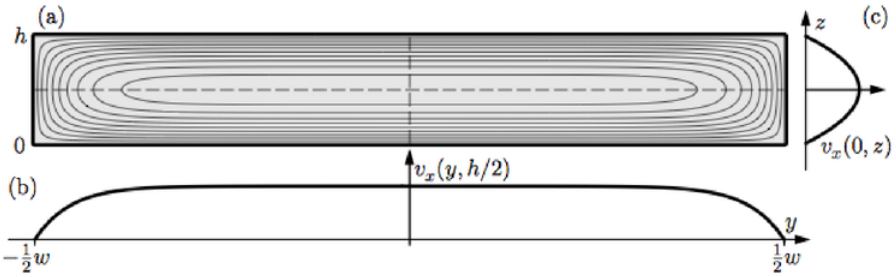

Figure 2.1: (a) The contour lines for the velocity field $v_x(y, z)$ in a Poiseuille flow across a channel with a rectangular cross section. Each contour line increments 10% of the maximum $v_x(0, h/2)$. (b) A plot of $v_x(y, h/2)$ (c) A plot of $v_x(0, z)$. Taken from Bruus.

Poiseuille flows or Hagen-Poiseuille flows are pressure driven steady state flows in a channel. This type of flow is characterised by fluid along a long, straight, and rigid channel with a pressure difference at the ends that drive the liquid. Understanding this type of flow is one of the first steps to handling liquids in lab-on-chip devices as shows what the velocity field across the cross section will look like in a controlled setup. Poiseuille flows have been studied along channels of various cross sections. To find the velocity fields across a channel can be quite difficult especially for unconventional cross sections. The velocity field is determined by calculating the velocity component across the cross section which exists as a vector quantity, $v_x(y, z)$, along the pressure gradient that changes along the unit vector along the x axis, e_x. From this the flow rate as a function of the velocity field can then be divided across the cross sectional area for various change in pressure, Δp. The LOC setup used for the study in this paper use channels with a rectangular cross section. Poiseuille flows for such channels do not have analytical solutions due to its shape, however a Fourier sum can be used to represent the solution. After solving for the velocity field using this Fourier sum the velocity profile can be given by:

$$v_x(y,z) = \frac{4h^2\Delta p}{\pi^3\eta L}\sum_{n,odd}^{\infty}\left[1 - \frac{cosh(n\pi\frac{y}{h})}{cosh(n\pi\frac{w}{2h})}\right]sin\left(n\pi\frac{z}{h}\right) \tag{2.6}$$

The velocity field can then be integrated to find the flow rate Q across the area:

$$Q = \frac{h^3 w\Delta p}{12\eta L}\left[1 - \sum_{n,odd}^{\infty}\frac{1}{n^5}\frac{192}{\pi^5}\frac{h}{w}tanh(n\pi\frac{w}{2h})\right] \tag{2.7}$$

Or the following approximation can be used with an error of 13% when $h = w$ down to 0.2% when $h = w/2$.

$$Q \approx \frac{h^3 w\Delta p}{12\eta L}\left[1 - 0.630\frac{h}{w}\right], h < w \tag{2.8}$$

The variables used in the equations above were channel height h, channel width w, pressure difference along channel length Δp, viscosity of the fluid η and length of the channel L.

An understanding and visualisation of Poiseuille flows is the first step in understanding the flows velocity profiles across a LOC devices. By mapping out these flows it is easier to discover how particles will move around in these flows and the relative velocities between them.

2.3.2 Hydraulic Resistance

The hydraulic resistance is a quantity that the interaction between channel geometry and the fluid flow. It can be used to find the pressure drop, ΔP, across along a straight channel of constant flow rate Q.

$$\Delta P = R_{hyd}Q \tag{2.9}$$

Devices that use rectangular input and output channels need to control flow rates and collect particle streams. So calculating this quantity is important for setting up a device, the device used in this paper uses rectangular channels so knowing the hydraulic resistance can identify the device particle size cut-off points. The shape of the channel that is being observed determines the hydraulic reistance R_{hyd}. Channels of rectangular cross-section do not have an analytical solution for R_{hyd}, however an approximation of the solution can be found using the Fourier transform found by Bruus that was detailed

in the Poiseuille version. The equation simply separates the differential pressure from the flow rate term to give R_{hyd} as:

$$R_{hyd} = \left(\frac{h^3 w}{12\eta L} \left[1 - \sum_{n,odd}^{\infty} \frac{1}{n^5} \frac{192}{\pi^5} \frac{h}{w} tan\left(n\pi \frac{w}{2h} \right) \right] \right)^{-1} \tag{2.10}$$

This approximates to:

$$R_{hyd} = \frac{12\eta L}{1 - 0.63(h/w)} \frac{1}{h^3 w} \tag{2.11}$$

Where η is viscosity of the fluid, h is the channel height and L is the channel length. [10] When determining the flow rate given a pressure or the pressure difference in long channel hydraulic resistance can be used.

2.4 Particle Migration in Microfluidics

2.4.1 Viscous Drag on spherical particles

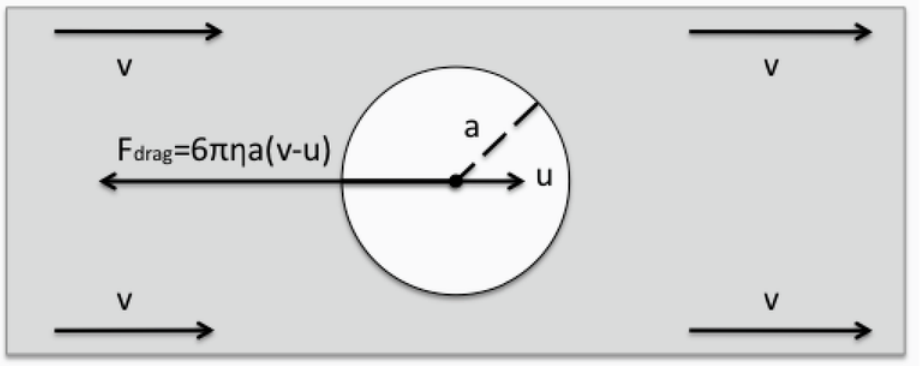

Figure 2.2: The viscous drag force F_{drag} on a spherical particle with radius a, in a Stokes flow where the liquid viscosity of the flow is η travelling at velocity v.

Viscous drag forces are applied to particles when a viscous fluid flows past it. The drag force is the calculated shear stresses on the particle surface by a viscous fluid flow. This drag force, F_{drag}, can be generalised by the expression:

$$F_{drag} = -6\pi\eta a(v - u) \tag{2.12}$$

Where μ is fluid viscosity, a is radius of the particle and u is the velocity of the particle and v is the velocity of the fluid if the particle was not present. This drag force at low Reynolds numbers is the force that most strongly affects the behaviour of the particle. A particle will not however have inertial movement from this force as the fluid stops acceleration of the particles in Stokes flows due to the collisions between it and the molecules of the liquid. Due to this phenomenon particles will move at the velocity of the fluid and should follow streamlines quite strictly at low flow rates. It then becomes easy for observing when external forces are used to act on the particles causing them to accelerate or cross streamlines which is necessary for understanding and testing separation techniques [11]. Even though it is easy to analyse particles in low Reynolds number flows, in real world applications separating particles at low flow rates is an unrealistic practice. To get to a higher more acceptable throughput of particles the Reynolds numbers need to be approximately 1 to make it viable in the field. However, at that point the inertia of the particle and the velocity field of the fluid flow can begin to affect the particle as vector velocity, u, of the particle increases causing the particles to move across streamlines changing their trajectory if viscous drag does not balance these forces.

2.4.2 Particle Migration at High Reynolds Numbers vs Low Reynolds Numbers

The Reynolds number is a common factor that describes the flow of a system. For low Reynolds numbers, Re $\ll$1, particle migration is easy to define and has been a focal point of a lot of literature in microfluidic. This is due to the heavy simplification of the fluid flows due to removal of velocity vectors making these flows easy to analyse and mathematically model. In these flows sometimes referred to as creeping flows all the particles move at the same pace as the fluids average velocity due to viscous drag force pulling the particles along streamlines [10].

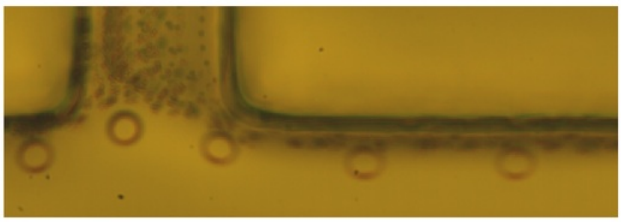

Figure 2.3: The focusing of particles at low Reynolds numbers to near the channel wall at Re=0.01

At lower Reynolds number flows the distribution of particles is important, especially for separation processes as it will usually be the determining factor to deciding the path of the particle. Generally this distribution will be random dependant on how the suspension enters the flow [15]. Initial particle position at low Reynolds number can be controlled so that the distribution of particles will focus on a certain area of the flow to direct particles on to a particular streamline for separation processes. This was done in some of the initial testing of the device where a buffer solution was used to push particles to the channel wall seen in Fig.2.3. Controlling the distribution of particles and the particle paths are the main properties that change with Reynolds number as the inertial effects on the particles come into effect.

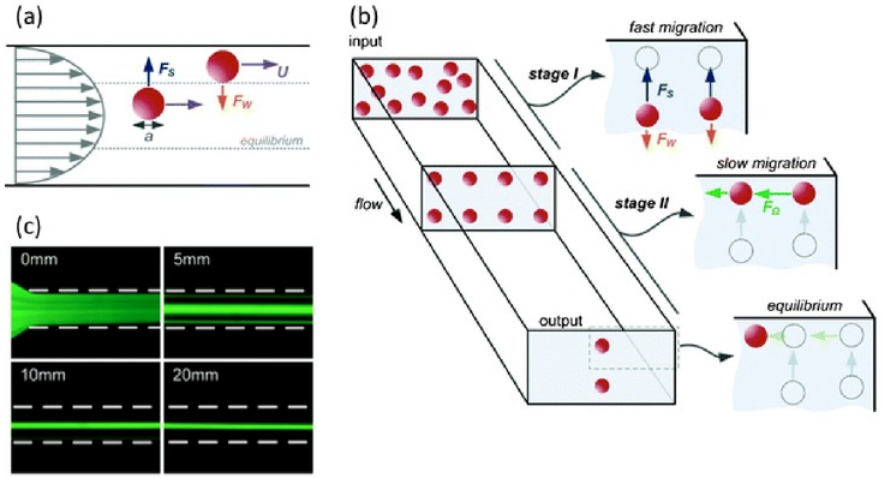

Figure 2.4: (a) The shear induced lift force, F_s of particles experienced at the peak of the velocity field and the wall induced lift force, F_w on the particle. The equilibrium line shows where the forces balance. (b) The migration of particles along a rectangular channel where stage I shows the initial movement to the edges and stage II shows the secondary movement towards the centre of the longer sides of the channel. (c) Images of fluorescent 7.32 μm particles travelling down a 25μm $\times$ 50 μm microchannel at Re = 70. [22]

Particles in low Reynolds number flows will follow streamlines closely unless external forces act upon them, this makes it easy to determine the paths they take. When inertial forces begin to act on the particle approximately when Re $\approx$ 1, the motion of the particles can change due to the shear induced lift forces on the particles and the streamlines that begin to develop into vortices called Dean flows [12]. Along flows in micro-channels of various cross sections, neutrally buoyant particles have been studied at higher Reynolds numbers. These lift forces can be seen in any bounded flow, as Reynolds number increases a wall-induced lift force, that acts to push particles away from the wall

coupled with a shear induced lift, that pushes particles towards the wall leads to particles migrating across streamlines laterally to the flow direction [12]. Depending on the shape of the cross section particles will distribute themselves differently but for the purposes of the device used in this paper, channels with rectangular cross sections will be the focus.

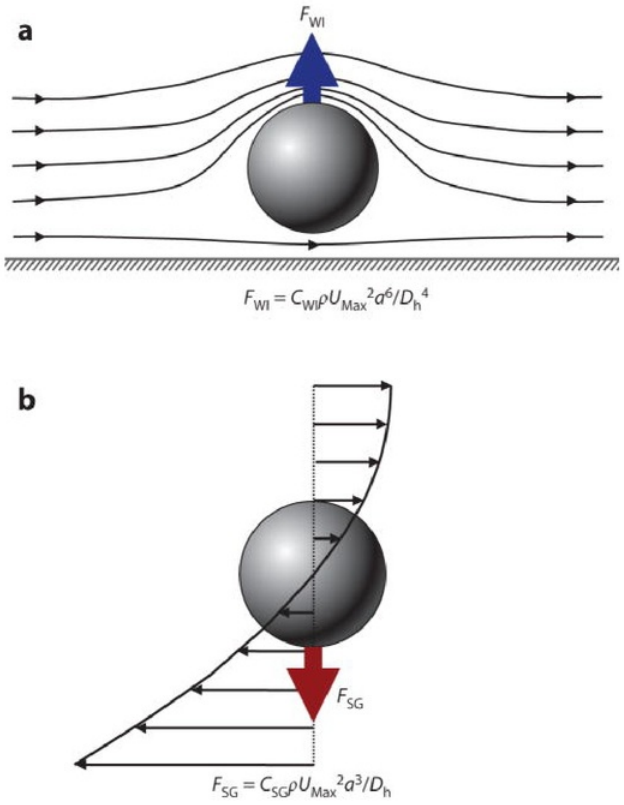

Figure 2.5: (a) The wall induced force, F_w on the particle and the distortion effect it has on the surrounding flow. The pressure build up on the wall causes the constricted flow to push the particle away from the wall b)The shear induced lift force, F_s of particles and the distortion effect it has on the surrounding flow. The relative velocity on each side of the particle causes the particle to move away from where the parabolic velocity profile is largest.

The lift forces on the particles in microchannel flows are caused by the vortices around the particle surface from the flows velocity field causing the particles to migrate towards the channel walls. Particles closer to the centre of the channel will experience a shear induced lift, F_s due to the different flow velocity surrounding the particle. The scaling factor of this force is due to the size of the particle and has been found to be

$F_s \propto a^2$. When these particles get close to the wall vortices in the opposite direction of the shear induced lift force moving the particle away from the wall. This force is more strongly dependant on particle size but also depends on the distance from the wall δ, this force scales as $F_w \propto a^3/\delta$ [12] [22].

Studies into this particle migration shows that the net lift force, F_L, is an equilibrium of these two effects and as such has a correlation to particles of diameter a, in a channel of hydraulic diameter D_{hyd}, scaling such that $F_L \propto a^4$. The theoretical calculation proposed by Asmolov, introduced a non-dimensional lift coefficient, C_L, to calculate F_L as a function of Reynolds number, the shear rate of the particle, $G = 2U_f/D_h$ (where U_f is average flow velocity and D_h is characteristic length of the channel) and the fluid viscosity, ρ [22] [18]. The theoretical calculation was as follows:

$$F_L = C_L G^2 \rho a^4 \tag{2.13}$$

The same parameters are similarly used for the shear and wall lift components of that equation given by:

$$F_w = C_L \rho U_{max}^2 a^6 / D_h \tag{2.14}$$

$$F_L = C_L \rho U_{max}^2 a^3 / D_h \tag{2.15}$$

These inertial lift forces may be useful for separation techniques but it should be mentioned that the focusing of particles occurs at relatively high Reynolds numbers over a particular distance before migrating to a final position. Fig.**??**(c) shows the inertial focusing of particles in a microchannel with a rectangular cross section where the particles focus on the longer sides of the cross section at high Reynolds numbers. This movement of particles may be able to collect particles to streamlines for continuous flow filtration as the particles will be at controllable equilibrium points in the channel dependant on its dimensions. When a mixture of different sized particles are in these flows the movement of the varying centrelines of the particles should be able distinctly separate the particles as the distribution of particles is less random than at low Reynolds number flows. These effects may play a role in the observations at moderate Reynolds number however the effects will be limited due to the small distances between the inputs and outputs of the device used in this paper.

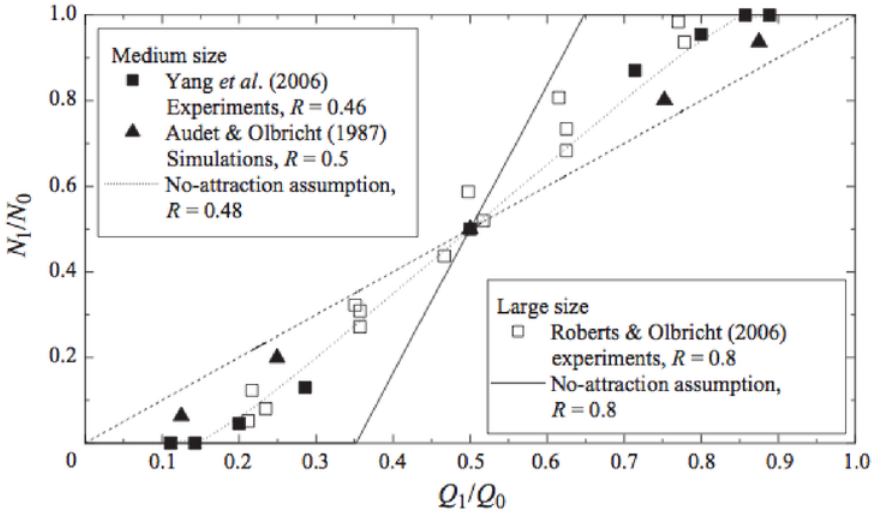

Figure 2.6: Taken from Doyeux et al. paper, this graph shows the previous results from Audet & Olbricht; Ditchfield & Olbricht; Roberts & Olbricht; Yang et al.; Barber et al., where homogenous distribution of rigid spheres are separated at a symmetrical Y-shaped bifurcation. The data compares the fraction of particles to the particle input, N_1/N_0, and the flow rate distribution of the inlet to one of the outlets, Q_1/Q_2. [15]

2.5 Particle separation at bifurcation at low Reynolds numbers

There have been many studies on the particle flow at bifurcations of different geometries at low Reynolds numbers. Most of the studies are done at symmetrical Y-shaped bifurcations in channels with square cross sections. These devices look at the correlation between the flow rate output and the separation of particles. The distribution of the particle separation in these experiments were analysed by comparing the ratio of an output branch to the input branch flow, Q1/Q0, to the number of particles down the output as a fraction of the total particle input, N1/N0. In each study the Zweifach-Fung effect was observed as when the output flow rate ratio was less than half ($Q_1/Q_0 < 1/2$), then the number of particles observed travelling down the outlet was much smaller ($N_1/N_0 < Q_1/Q_0$).

Doyeux et al. highlights that through these previous experiments there still exists some attraction to the low flow rate branch as the cutoff size is not greater for higher flow rates, especially in cases where particles with radii of 0.8 of the channel area and the fraction of the flow rates was less than 0.35. Here the fluid separating line theoretically lies further down the channel than the particle radius, if there was no attraction to low

flow rate branch then no particles would flow down that branch. The results from Fig.2.6 show that this is not the case because a number of particles do travel down the low flow rate branch crossing the fluid separating line as the radius of the particles increase. So even though the Zweifach-Fung effect is observed this means that the particle path was influenced by some other factor. The problem with assumptions made in previous experiments was a disregard for the initial position of the particles. Depending on the initial position of the particles they will either move directly into the high or low flow rate branch, the trajectory of particles closer to the fluid separating will show an attraction to the low flow rate branch before the particle follows streamlines moving into the high flow fate branch [15].

The relationship between the flow and the particle movement can be described using the pressure difference between the walls of the channel. A particle in an asymmetrical flow will be determined by the pressure difference between the particle and the fluid separating line between the different flows, the particle will move towards the low pressure systems along the channel. This easily explains the movement into the high flow rate branch when the particle reaches the bifurcation because the high flow rate branch is always under low pressure and so the attraction is clear. The attraction to the low flow rate branch is more difficult to explain but can be attributed to the pressure difference between the front and back of the sphere in the channel before reaching the bifurcation point, $\Delta P = P_0\text{-}P_i$ in Fig.2.7(a), where the lower pressure difference would be where the particle would be attracted to. Doyeux et. al points out that this effect causes particles to distribute themselves in a way that favours the low flow rate branch before the particles reaches the bifurcation. The particle must overcome this initial attraction before moving into the high flow rate branch at the bifurcation [15].

From research into microfluidics theory devices in research papers have used hydrodynamic filtration at bifurcations to separate particles by size. In Inglis's papers an LOC device that splits an input fluid stream into two output streams, where one one stream carried out filtered large particles and the second stream contained small particles. Branch flow filtration takes advantage of the idea that small particles will flow into the branch flow as they can move closer to the boundary layer of the flow. Yamada and Seki's explain that if the particle centre line path, a particles radius away from the sidewall, is large it will not be able to go through a side channel as flow path of these larger particles will tend to follow a higher flow rate channel [17]. As the flow rate increases the tendency for these particles to go up the branch flow will increase dependant on the size of the particle. Inglis's device highlights the reason why continuous flow filtration using bifurcations is advantageous for the purpose of filtration, the reason being that it is possible to increase branch length which in turn increases the hydraulic resistance of the branch reducing fluid flow. By varying the hydraulic resistance this idea that smaller particles will follow streamlines at smaller flow rates could be tested [16]. The results of these hydrodynamic filtration experiments showed successful results where Yamada et al was able able to separate polymer particles into 1.0, 2.1and 3.0 μm particles with 60

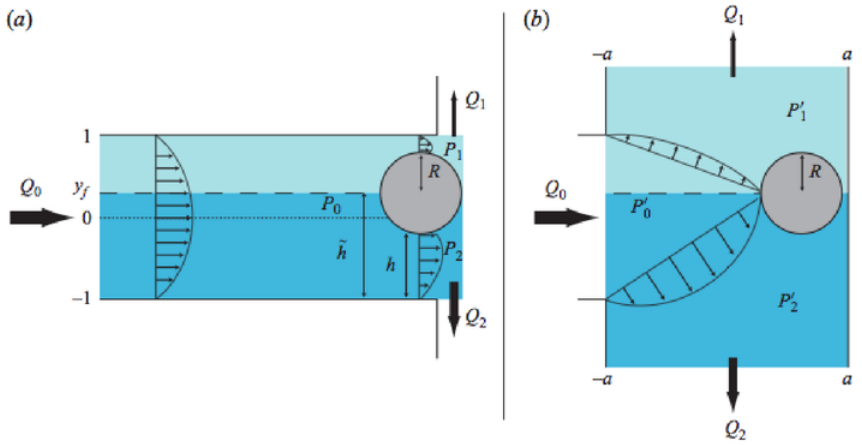

Figure 2.7: These diagrams show how the pressure difference affects the migration of particles at channel bifurcations in asymmetrical flows. (a) The entrance of the bifurcation showing attraction to the towards the low flow rate branch as $P_1 < P_2$. (b) The particle at the bifurcation wall showing the attraction to the high flow rate branch as $P'_1 > P'2$. [15]

percent recovery rate. Inglis used a alternative device that concentrated on sharper cut off size, this allowed for comparatively higher filtration ratios by using multiple branches of varying resistances to increase the separation of smaller particles.

2.5.1 Particle Separation using Moderate Reynolds Numbers

There are some research into LOC device geometries that can take advantage of the moderate Reynolds number flows as a way to cause particles to move onto separate streamlines. Devices that can use soft inertial forces, where Reynolds number of the flows are around 1, can cause a noticeable displacement of particles, moving the particles onto different streamlines. The device in Fig.2.8 shows a device that uses these soft inertial forces as a way to separate bacteria from blood cells. The net inertial force of the larger particles commonly observed in geometries with sudden expansions or turns particles are used to make a device that uses the momentum of these particles will separate [**?**]. These forces are usually tied to the particles Reynolds number, R_p, which shows information of how the shear and viscous forces act on the particle. For spherical particles with radius, a , in flows with velocity, V, density, η and characteristic channel dimension length, L the particle Reynolds number can be found using the following formula.

$$R_p = Re\frac{a}{L^2} = \frac{\rho V a^2}{\mu L} \tag{2.16}$$

The separation between the smaller and larger particles in the device increased as this particles Reynolds numbers increases due to the shear stresses relative to the velocity. The device managed to have a high throughput of blood cells separated from bacteria. This device shows how inertial effect can be used in conjunction with certain geometries to separate particles by size.

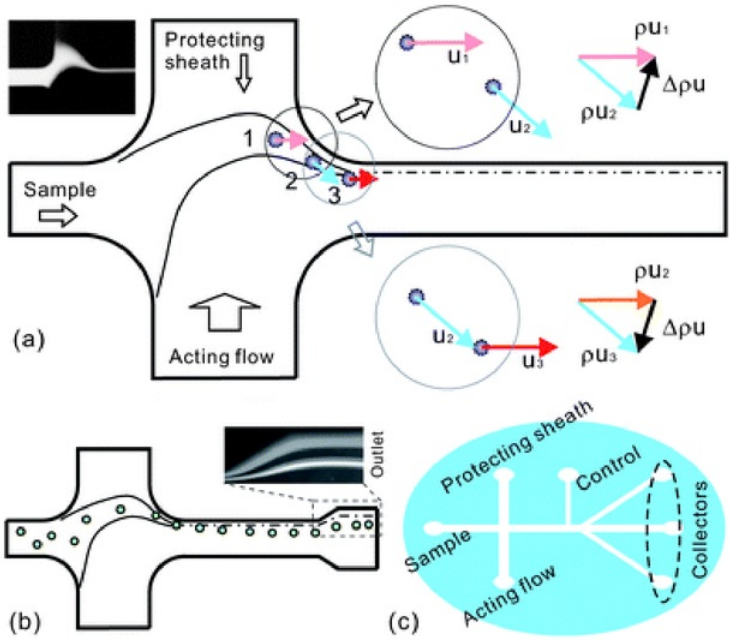

Figure 2.8: The concept of soft inertial separation and schematics of device design: (a) the schematics the inertial effects used to move particles into different streamlines (b) the schematics of the particle separation in the device. The right corner shows an example of the larger particles deflecting from the sample flow at the expanded outlet (c) the schematics of the device design. [?]

Chapter 3

Approach and Methodology

3.1 Introduction

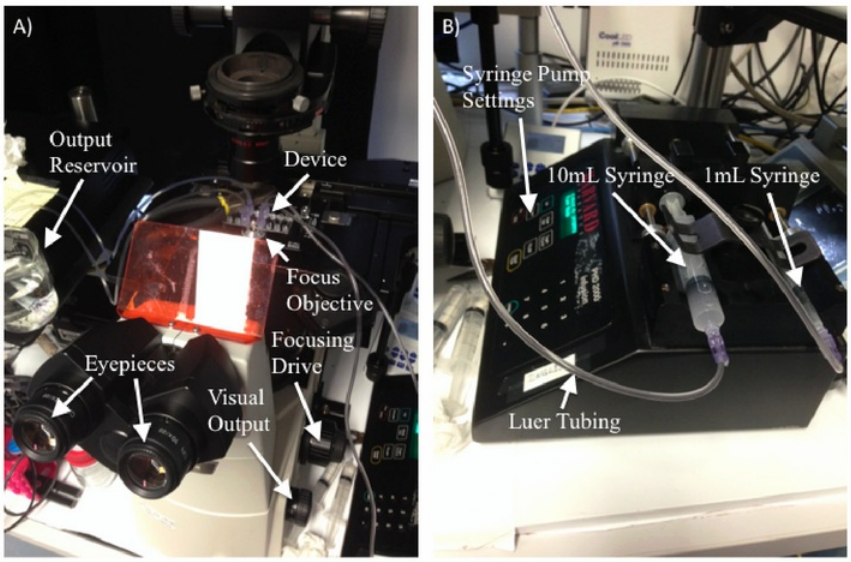

Figure 3.1: A) Labelled photograph of device rigged to inverted microscope. B) Syringe pump setup.

The behaviour of rigid micron scale spherical particles of different radii was studied along a microchannel thats splits into a two channel bifurcation. In first hand studies of the behaviour of suspensions in microfluidics various pieces of equipment and a

designated LOC device are usually required to control and observe the way that the fluid acts on the particles for different geometries. The equipment and experimental setup used to carry out this study are outlined in this chapter.

3.2 Equipment

3.2.1 Inverted Microscope

An inverted microscope is a complex piece of equipment required for the analysis of any subject at the micron scale. The microscope takes magnified images from underneath the subject placed on a platform above an objective lens and projects the images onto a visual output, usually the eyepiece or to a camera attached to the side of the microscope. The receive good visual data from an inverted microscope it is necessary to adjust the settings so its possible clearly see the part of the subject that requires focusing. The following process is used to focus the images from a micro-scale channel bifurcation on an LOC device.

1. Turn on the light switch on the microscope. Adjust the brightness to low before looking through the eyepiece.
2. Adjust the distance between the eyepieces on the binocular tube by rotating them toward or away from each other. When the distance between the eyepieces matches the distance between your pupils, you will see images in both eyes.
3. Start by focusing on the device with lower focus objectives usually a 10x objective lens or lower. The objectives can be changed by rotating the objective nosepiece so that the particular objective you wish to use is set under the device.
4. Focus the image seen in the eyepiece to the required distance through the subject by turning the focusing drive on the microscope. The coarse drive can be used to find the channels of the device. The smaller knob, the fine focusing drive can be used to determine the exact distances in microns that the focus is at along a channel. If higher magnification is required change the objective lens to one with higher magnification, so see particles along the 50 μm channels used in this particular LOC device objectives of 20x and 40x were used to clearly see the particles.
5. Focus the image of the centre of the channel by finding where the edge of the wall just goes out of focus using the fine focusing drive wheel.
6. Record where the wall edge is by using the corresponding number that the wheel aligns to.

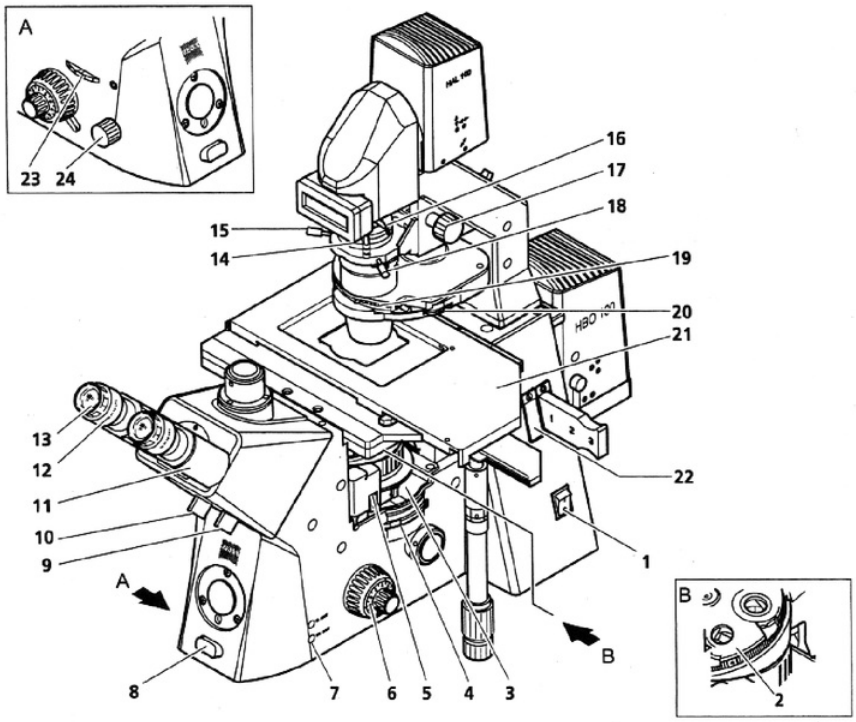

1 On / Off switch
2 Objective nosepiece
3 Compartment for slider Analyzer
4 Setting wheel for Optovar turret
5 Reflector turret
6 Focusing drive coarse / fine
7 HAL on / off switch
8 Toggle switch for illumination intensity
9 Turning or sliding knob for vis / doc beam splitting
10 Turning or sliding knob for Bertrand lens and manual shutter
11 Binocular tube component
12 Setting ring of the eyepiece
13 Eyepiece
14 Polarizer D with 2-position filter changer
15 Centering screw for condenser
16 Setting lever for luminous-field diaphragm
17 Setting knob for vertical adjustment of the condenser
18 Centering screw for condenser
19 Turret disk of condenser
20 Setting wheel for aperture diaphragm on the condenser
21 Microscope stage
22 Compartment for aperture diaphragm slider
23 Setting wheel for Sideport
24 Setting knob for Frontport / Baseport

Figure 3.2: A) Labelled diagram of the inverted microscope. [28]

7. Turn the fine focusing drive wheel to the other wall edge taking into account the number of rotations and the final number the wheel aligns to. The distance that is rotated will be distance from the top to the bottom of the channel.

8. Half the channel height found and rotate the fine focusing drive wheel by that amount so that the image displayed rests at the centre of the channel.

Images from the microscope can change according to how the subject of the microscope is illuminated. To achieve good illumination the procedure developed by August

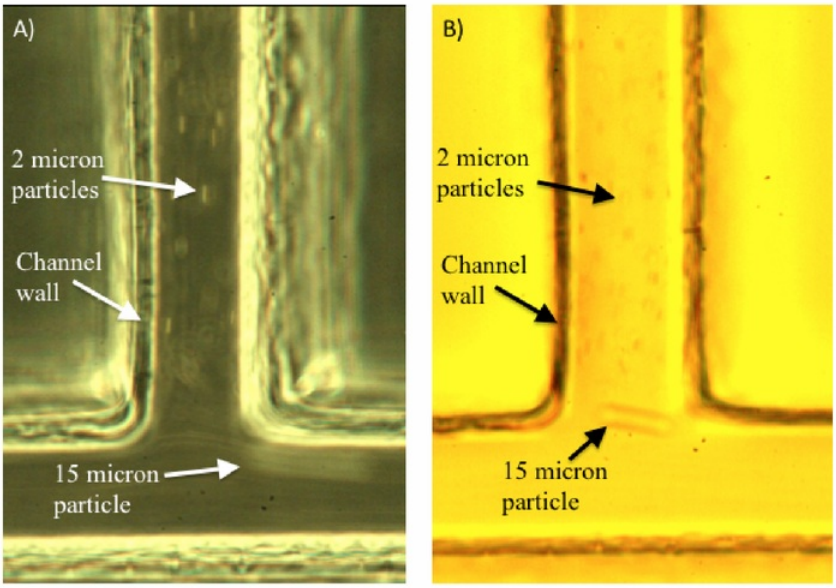

Figure 3.3: A) Fluid flow of bead suspension with phase contract on from a 20x objective lens. B) Fluid flow of bead suspension with no phase contrast. Both flows have been recorded at Re=1

Kohler called Kohler illumination can be used, this technique results in little reflection or glare and minimal sample heating. The steps required to use Kohler illumination are as follows:

1. Turn on the light switch on the microscope. Adjust the brightness to low before looking through the eyepiece.
2. Find the two irises in the illumination path of the microscope from the light source, the irises will have sliding knob that can open and close the .
3. Close the top iris (called the field iris) so that you can see its outline in the eyepiece.
4. Open the bottom iris (called the condenser iris) fully.
5. Focus the condenser iris to the point where the light almost disappears.

Along with Kohler illumination it is possible to change the image seen by using a phase ring in the condenser iris that cause an effect called phase contrast. Phase contrast is a setting on the microscope that changes the brightness of the subject by

creating interference between scattered and background light. This technique can be useful in creating contrast between particles of different focus sometimes making the particles easier to see. An example of the difference between phase contrast and normal illumination settings can be seen in Fig.3.3.

3.2.2 High Speed Camera

To record videos of particles travelling in microfluidic devices the use of a high speed camera is highly necessary. Particles will travel across the image taken by the inverted microscope spanning 466 in less that 0.005 seconds for Reynolds number more than 0.1, a normal camera with 25 fps that takes 0.04 seconds between each frame would not be able to capture the particle moving along the channel. The phantom high speed camera records at sample rates up to 2600 fps which allows for 0.38 milliseconds between frames which can track the particle at approximately 10 points across the image. This does make it difficult to track individual points of particles with the high speed camera when the Reynolds number of the flows exceed 1 at that point it will only be possible to track the particle path by changing the camera settings so that the exposure time of the camera is increased.

The camera settings can change multiple aspects of how the video will look after recording. To see clear particles at a single point the exposure time needs to be set as short of possible however decreasing the exposure time makes the film darker. Increasing the exposure time can cause the camera to capture an elongated oval shape of the moving path of the particle this can be a desirable effect especially when the speed of the particles are too high to capture in still frames. The exposure time can be set to a maximum of the frame rate speed. The number of frames per second can be changed to a maximum of 2600 fps, this requires the image resolution to change so that the shutter speed decreases to match this frame rate. The maximum resolution achievable by the camera in 1920×1200. Videos up to 3 seconds are able to be stored in the camera and can be saved onto a computer or hard drive. The 3 seconds of memory space for the videos can be partitions so that there exist multiple videos that has a length of 3 seconds divided by the number of partitions. To record the video a trigger button in conjunction with a sliding bar that sets how much time before and after the trigger you wish to record. This feature can be especially useful for high speed videos as the delay between the visual stimulus and the trigger point can be quite high. A combination of these settings will need to be set in order to get the wanted video results. Videos taken by the high speed camera used in this paper were recored at 1300 fps with a 300 μs exposure with a resolution of 1920×1200.

To be able to see images through the high speed camera at most settings, a large amount of light is needed by the camera so that it can take videos at a higher frame rate at high resolution and low exposure times so if initially there is no visuals on the screen increase the brightness of the lamp then adjust the settings for the desired effect and

length of the video for later particle tracking.

The high speed camera needs to be attached to the the microscope with a microscope lens attachment that is screwed into the side of the microscope. This high speed camera requires an ethernet cable adapter that needs to be connected to the the computer. To be able to use the camera on a computer you will need to change the IP address to match the cameras by going to settings > network preferences > network internet > network and sharing centre > change adapter settings > ethernet, left click on ethernet and go to properties, click on TCP/IPv4 > properties > choose IP address and change to 100.100.100.1 with subnet mask 255.255.0.0. The camera will then be ready to be accessed by the Phantom Camera Control software (PCC2.8) where the settings detailed before can be set.

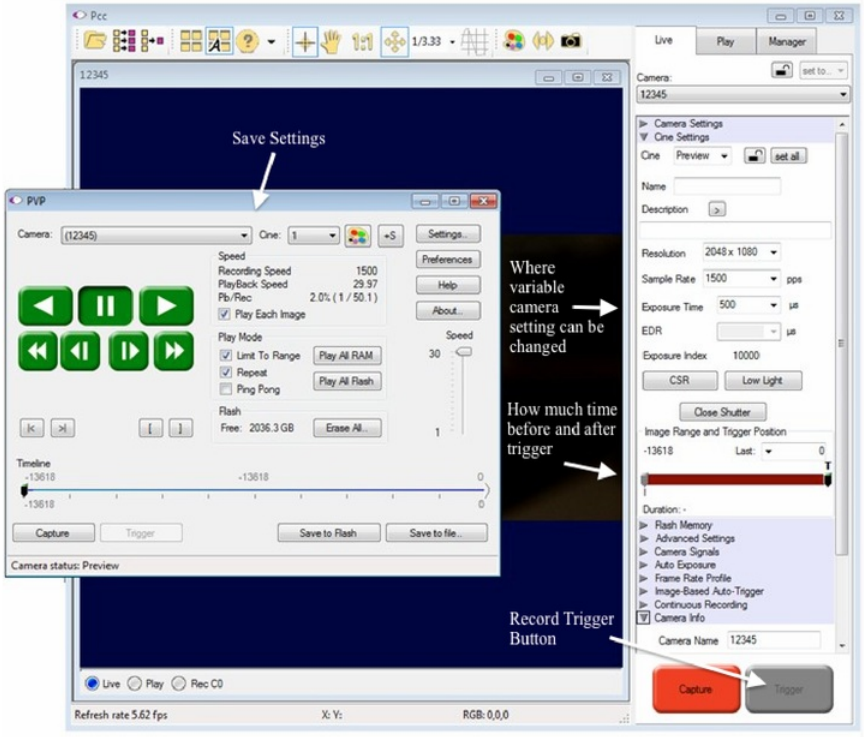

Figure 3.4: Phantom Camera Control settings from the PCC2.8 Software.

3.3 Device Fabrication

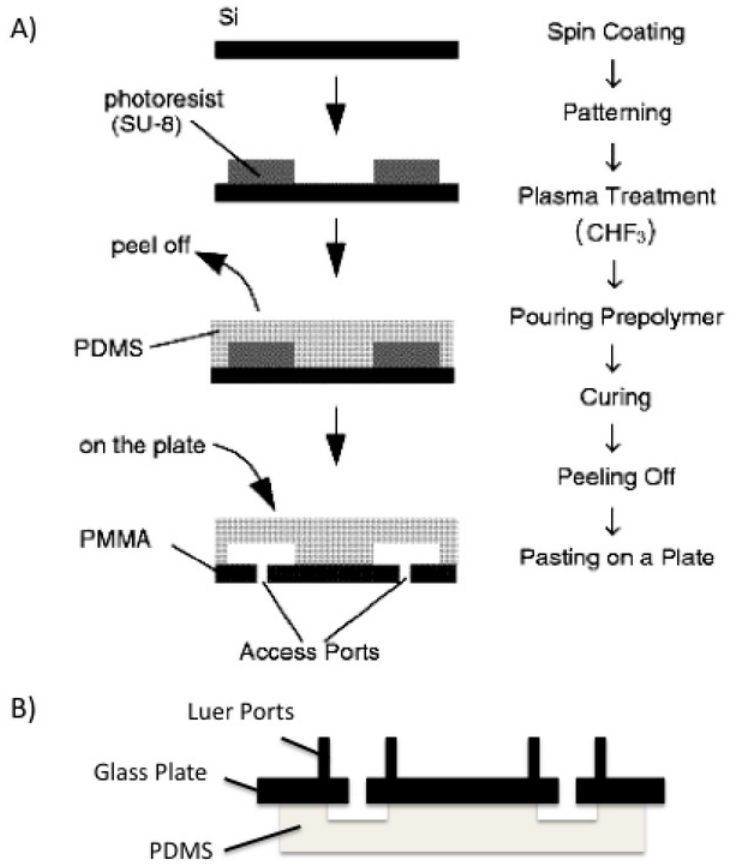

Figure 3.5: A) The average fabrication process used to create PDMS synthesised microfluidic devices [23]. B) The cross section of the luer ports that are set of the the device lids used in this paper.

The device used in this paper is made of PDMS (polydimethylsiloxane), a common substance used in microfluidics as the elastomer is inexpensive, flexible and compatible with many optical methods of detection and glass. To create the microchannels in these devices a mould master made from a silicon wafer and the microchannel pattern photoresist is made, PDMS prepolymer is poured into this mould then cured. After curing the PDMS, now with the microchannel pattern inlaid on it, can be bonded to a flat plate usually a transparent material such as PMMA (polymethylmethacrylate) or glass where the ports used to inject fluid into are placed [23]. To bond the PDMS to the glass

is relatively simple as it can be attached with spontaneous adhesion to it if the surface is flat. The adhesion property that PDMS has is a reversible process and makes it easy to change PDMS chips however at certain pressures from liquid flow rates, around 5-10 psi, the device can leak and the Vanderwaals forces between the PDMS and glass break. To avoid this from happening an irreversible seal can be created between the two surfaces by exposing the surfaces to oxygen plasma. Silanol groups that appear on the surfaces of the PDMS and glass after being exposed to oxygen plasma create Si-O-Si covalent bonds after curing at room temperature or in an oven. Devices that undergo this process can withstand 30-50 psi of air pressure and are not easily separable [23] [24]. Pressure build up in these device can also lead to deformation in the PDMS chip changing the dimensions of the microfluidic channels. The glass lids used in this device have 6mm diameter Luer ports. Luer ports take Luer taper connections, standardised small scale fluid fitting for laboratory instruments, made for leak free connections between male-taper fittings and its female counterpart. Due to the size of the tubing that was required by the device the sample size of the fluid was larger than required. It is recommended that more flexible tubing of small diameter is used to reduce the required sample size and if possible change the port type from a standardised Luer taper port to standardised ports with smaller fittings. The PDMS is centred on the device by milling channels 3 μm deep from the Luer ports to the input ports of device. The microchannels set into the PDMS have rectangular cross sections 50 μm wide and have a depth of 200 μm.

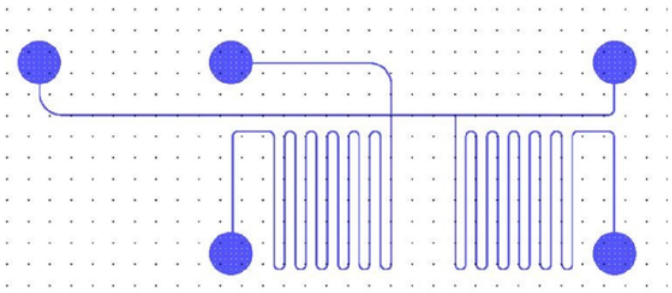

Figure 3.6: The diagram shows the LOC device that will be used for the project. On the left side three inputs for controlling input flow rates and on the right to outputs one for main channel and another for branch flow output from the bifurcation.

3.4 Device Design

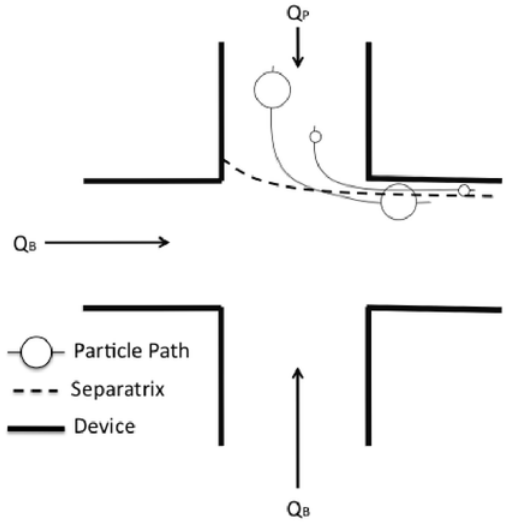

Figure 3.7: The three inputs for controlling input flow rates and guide the particles towards the channel wall with the buffer solution.

The device was designed and put together by David Inglis for the purposes of this experiment, which included the preparation of the PDMS device and the attachment to the glass lids.

The device was required to analyse the motion of particles at a bifurcation so it needed to have the two output channels placed perpendicular to each other for the main channel flow and the branch flow. The branch flow acted as a resistive channel that was designed to let 1-10% of the flow down down that channel whilst the main flow had 90-99% of the flow from the input.

To find the separatrix and the see the particles move around it particles needed to be pushed towards the wall in order for the particles of different sizes to follow different streamlines. Three inputs are used, one of the inputs is for a bead mixture of 15μm and 2μm to travel up whilst the other two input channels are for a buffer solution with only 2μm beads that pushes the larger particles towards the wall of the device so they follow particular streamlines whilst allowing the observation of the separatrix line. The channel used for placing beads in and the perpendicular channel have an increased hydraulic resistance, this resistance is used to allow the right concentration of beads to go into the device and to create a sharp cutoff at the resistive output branch.

To ensure constant input flows syringe pumps were used to inject fluid at specified flow rates. The ratio of the rate of injection of the buffer solution flow, Qb, to the particle solution, Qp was 10:1. This was achieved simply by using a 10 and 1mL syringe. This ratio of input flow rates was a necessary step to ensuring that particles would be near or touching the wall. The two output branches were linked to reservoirs of the same height to prevent a hydrostatic pressure gradient changing the direction of flow. If the heights of the reservoirs changed so the channels connected to the reservoir were elevated then those channels will have an increased pressure causing resistance in the flows making them slower, the opposite will occur in the reservoir is lowered. This may heavily influence the flow rates in the channel and should be noted when conducting microfluidic experiments where the pressure is not controlled using machinery.

3.5 Experimental Setup

3.5.1 Suspension Preparation

A suspension of particles was synthesised for use in the experiment. This fluid composition of the suspension was a mixture of glucose and water, this was done at 1:10 ratio so that the density of the fluid would be similar to that of the particles, which were made of polystyrene with a density of 1.05g/cm^3. This density was required by the fluid so that particles will be neutrally buoyant in the solution. Using the glucose and water mixture two solution of suspensions were made. One contained both 15μm and 2μ beads, the other solution that would act as a buffer solution contained only 2μm beads. The concentration of the beads used per 5mL of glucose water mixture was 200μL of 15μm beads and 40μL of 2μm beads in the first solution and the same concentration of 2μm beads in the second. Tween 20 was added to each solution to prevent clogging of the device, this was added at a ratio of 0.1:1000 between Tween 20 to solution volume. Before the solutions could be used in the device they were placed in an ultrasonic bath to ensure that particles don't clump together in the channel potentially clogging the device and ruining results. An example of these phenomenons are shown in Fig.3.8.

To accurately measure the correct quantities and concentrations of substances pipettes were used, when using a pipette ensure that the correct volume is set on the device using the adjustment wheel. With a clean pipette tip attached press the button on the end of the pipette and submerge the end of the tip into the required solution. Release the button and wait for the solution to be place into the pipette tip, this will take longer for denser liquids such as glucose. Then place the pipette tip over the container you will be mixing the solution into then hold down the button to release the solution. When finished with the pipette dispose of the tip by pressing on the tip ejector. A labelled diagram of a pipette is shown in Fig.3.9.

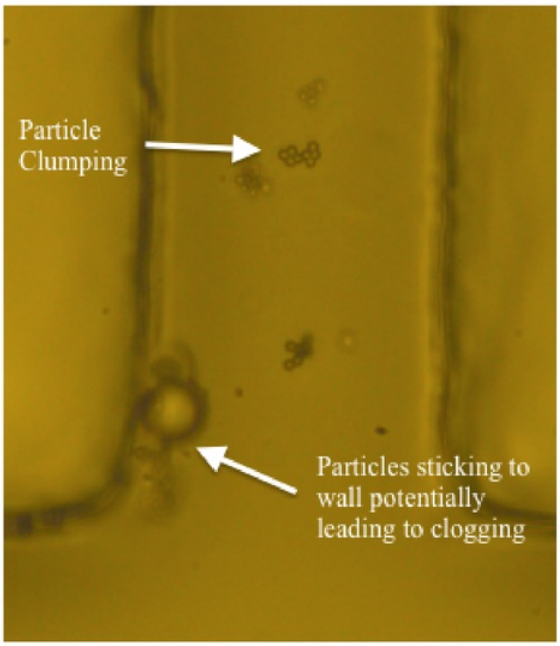

Figure 3.8: Initial tests where Tween 20 was not added to solutions and particle suspensions were not placed in the ultrasonic bath before running the device. This lead to both the clumping together of particles and clogging at various points along the channels.

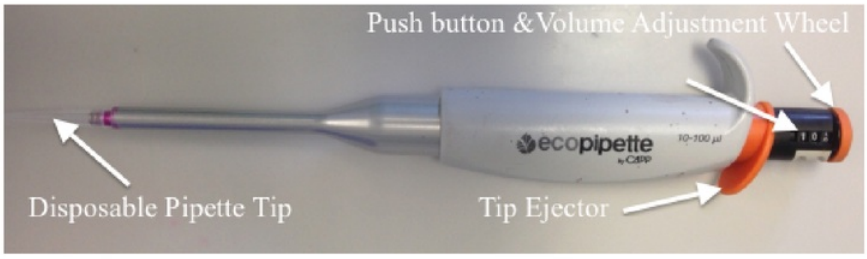

Figure 3.9: Annotated pipette diagram.

3.5.2 Device Preparation

Before running any microfluidics procedure the device needs to be cleaned so that dust particles, biological matter or beads that have settled in the device that are usually deposited there from previous tests, can be dislodged and taken out. To clean the device you can start by flushing the channels with 2-propanol this should kill any biological matter and some particles. The 2-propanol can be diluted with water so that the their

is 70% water and 30% 2-propanol. It is not recommended that devices with acrylic glass bonded to it should not be soaked in 2-propanol as it can potentially cause the glass to crack and frost near the channels making them hard to see. After flushing the channels with 2-propanol a detergent solution to flush the device a second time and can be used to soak the device. This is done with Extra MA Alkaline detergent diluted with water at a ratio of 1:100. The device channels should then be flushed a third time with clean distilled water. Check the device under a microscope to check if the any particles are still lodged in the device channels. If they are it may be necessary to part the device in an ultrasonic bath in a clean room then flushing the device again with distilled water.

After cleaning the device it is necessary to wet the device so that there are no air bubbles trapped in the device. On the LOC devices these bubbles are problematic as it causes the channels to be clogged as they usually span the entire cross section of the channel. So to remove these bubbles external pressure needs to be introduced to remove these bubbles. The first step to removing these bubbles is by injecting distilled water in the device. If bubbles are still trapped in the device then place the device in distilled water under a vacuum. Weight the device down in the vacuum device so that the device doest float on top of the water if possible. Leave the device in the vacuum for an hour, after that time has elapsed the device should have all the air bubbles removes.

Any time that liquid is injected into the device ensure the flow rate is slow enough not to cause pressure build up in the device as it can distort the channel geometry and causes leaks in the device.

3.5.3 Flow Rate Control

In this experiment micron sized spherical beads were passed through a bifurcation to observe the different streamlines of different sized beads. The two sizes of beads that were used were 10 and 2 micron in diameter. A syringe pump was used to inject a solution of glycerol and water of density 1.055kg/m^3 into three input flows Q1, Q2 and Q3 seen in Fig.**??**. The solution through input flow Q1 contained a mixture of 10μm and 2μm beads while the solution through input flows Q2 and Q3 only contained the glycerol and water solution. For the first set of results, Q2 and Q3 have equal flow rates that are 10 times the flow rate of Q1, this was done using a 10ml and 1ml syringe. The second set of results will be from flows Q1 and Q2 at the same flow rate ratio of 1:10 where Q3 will be plugged with back pressure to see if the liquid separatrix and particle path changes.

To calculate the Reynolds number proportional to the flow rate, the equation for flow rate across a channel of cross sectional area, A, with average velocity, V was used.

$$Q = VA \tag{3.1}$$

Table 3.1: This table shows the flow rate and velocity of the glucose water solution for Reynolds numbers between 0.01-0.09. This could be scaled for higher and lower Reynolds numbers.

Reynolds Number	Velocity (m/s)	Flow Rate (mL/min)
0.01	0.0084	0.005
0.02	0.0168	0.01
0.03	0.0252	0.0151
0.04	0.0336	0.0201
0.05	0.042	0.0252
0.06	0.0504	0.0302
0.07	0.0588	0.0352
0.08	0.0672	0.0403
0.09	0.084	0.0504

The velocity for the fluid flow was found by using the equation for Reynolds number (A.4), which is then substituted into equation 3.1 to determine the flow rate. A relative table for the values of Reynolds number, flow velocity and flow rate in the 200×50 μm channels are show in Table 3.1.

Chapter 4

Analysis and Results

4.1 Particle Tracking

The behaviour of spherical particles are studied near the bifurcations using videos of these particles at various Reynolds numbers. The videos allow for a two dimensional analysis of particles which can be tracked using the image processing program ImageJ. To track particles using this program an extension called MTrackJ needs to be added on the program as a plugin after installation this allows you to track the velocity and displacement of the multiple particles simultaneously from the same set of images. The time between each picture and the scaling of the picture from pixels to μm can be done in the image property settings so that a real data set can be extracted from these videos. The time between each frame will be determined by the speed of the video that is recorded, for the videos recorded in these results each frame was 0.77 milliseconds apart. Fig.4.1 shows the tracking of multiple particles using the software in the ImageJ program. These particles are tracked independent of each other with separate tracking IDs for referencing when processing data.

Data extracted from the particle tracking positions recorded from the video files recorded by the high speed camera has data such as the x and y positions of the point chosen with respect to the image dimensions, the velocity and the when a new position is reached with respect to the time the position is reached. It should be noted that the position of particles recorded by have an error of 4 μm due to manual selection of points where the pixel length is 4 μm. Some of this data has been represented using graphs in Fig.4.2 and Fig.4.3. The data captured in these figures are very useful for data analysis as well as a reference for future data collection. For example the data in Fig.4.2 shows velocity against the time from when the particles are initially tracked to where the tracks end. This shows the how many reference points can be gathered for certain velocities that the particles have along a channel as well as the complete time taken for a particle to

travel a measured distance. The other graph shows how the velocity changes as particles go through the channel past the bifurcation. The bifurcation lies 300 μm away from the x origin which lies on the further most right side of the picture in Fig.4.1. Looking at the velocity changing along the x axis shows how the velocity of the particle changes as it reaches the bifurcation and takes a path towards the main flow or the branching flow. This type of data was taken for various Reynolds number flows and compared.

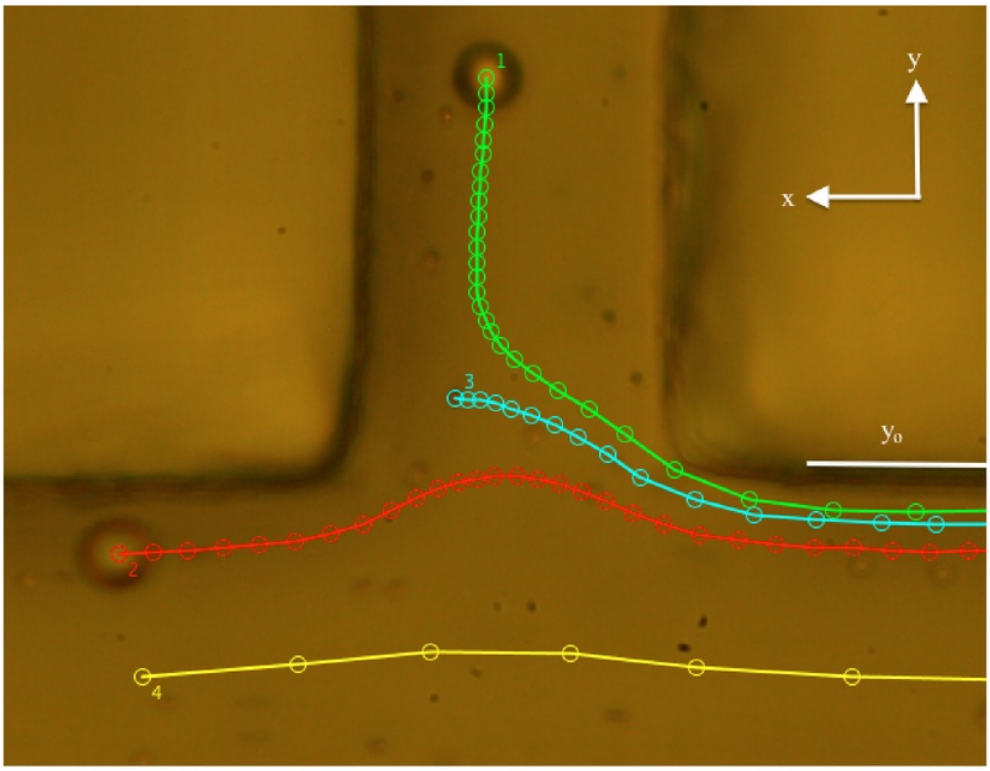

Figure 4.1: This is an image of four different particles that have been tracked. Tracks 1 and 2 show 15 μm at taking different paths near the separatrix, track 3 shows the movement of a 2μm particle at the separatrix and track 4 shows a 2μm particle at the centre of the channel.

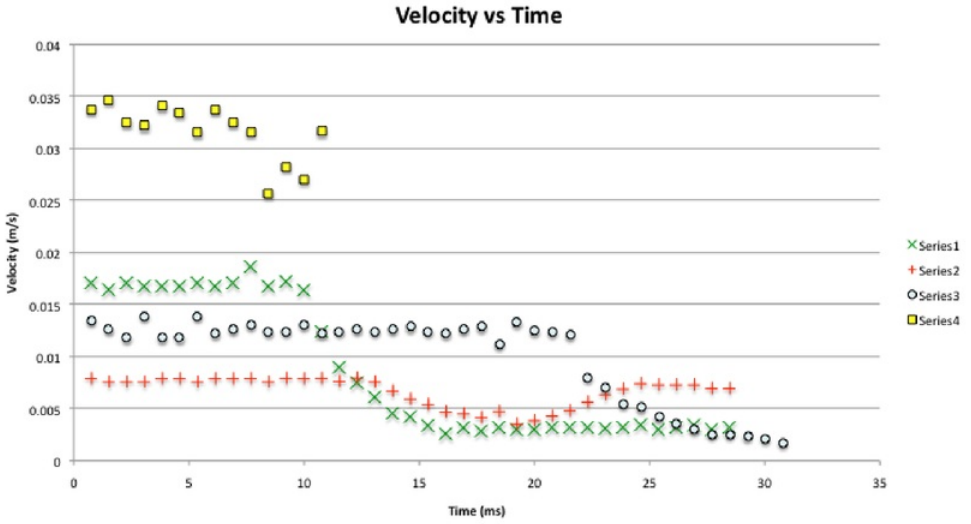

Figure 4.2: Plot of the data from Fig.4.1. The graph shows the velocity of the particles that were tracked against time.

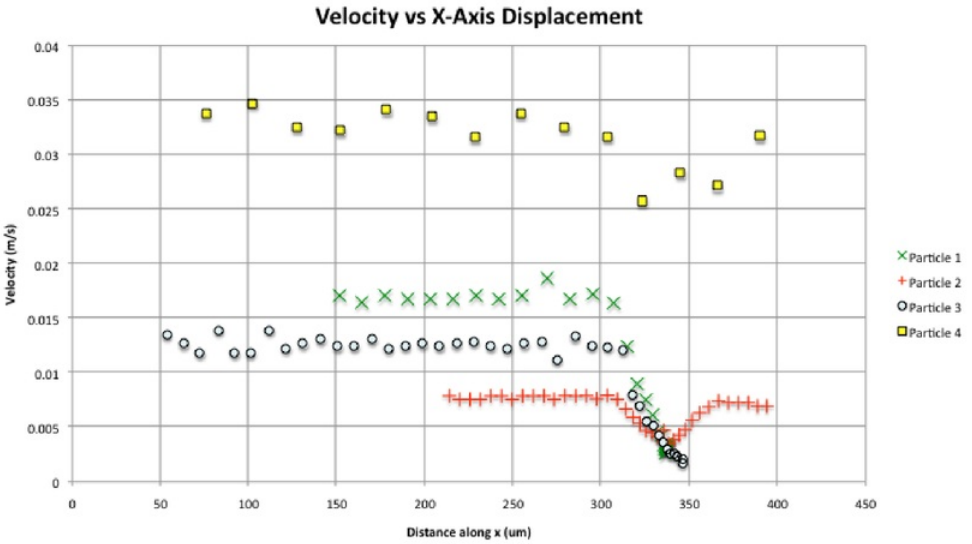

Figure 4.3: Plot of the data from Fig.4.1. The graph shows the velocity of the particles as the particles travel along the x-axis of the channel

4.2 Particles Recorded near Separatrix

In table 4.1, a comparison of some tracked 15 μm particles at different Reynolds numbers are shown. This table outlines some of the main results that need to be obtained in this paper which is the comparison of the fate of the particle with increasing Reynolds number. The fate of the particle is shown by defining the output flow that the particle moves towards, either the perpendicular branch flow or the main channel flow, where the flow rates in these channels are determined by the syringe pump input and the hydraulic resistances of the channels.

Information on the initial velocity of particles in the flow were used as a reference for flow velocities and the relative velocity of larger particles in these flows. The expected Reynolds Number flow rates that were originally pumped into the device were recorded as a comparison to the approximate experimental Reynolds numbers of the flow according to the velocity of 2 μm particles travelling at the centre of the flow. There was also an observed correlation between the initial particle position and Reynolds number as they increased.

The fluid separating line needed to be defined in order to correlate the centrelines of large particle with the separatrix boundary between the main and branch flow. Due to the asymmetrical velocity profile caused by the geometry of the channel bifurcation the separatrix lines that define the two possible modes of behaviour are not clearly identifiable but can be assumed to say located at the same distance if the fraction of flow rates into each channels stays the same. To find the separatrix boundary where the flow behaviour changes 2 μm particles were used to find the fluid separating lines as particles less than 3 μm diameter in size behave like fluid particles [15]. The secondary method used to check where the separatrix lies is by taking the data showing the fate of the particle with the changing initial position of the particle. From these two pieces of information the separatrix can be assumed to lie between 8.2 μm and 11.6 μm away from the wall near the bifurcation y_0, but closer to 8.2 μm which can be seen in path projections of the videos (Fig.4.4).

For the particles recorded, the fate of the particles was graphed against the initial position and Reynolds number to see probability trends in the data. The relationship between initial position and Reynolds number was graphed for reference.

Table 4.1: Table of 15μm particles tracked at various Reynolds numbers and the fate of the particle relative to the original particle position, y_p from the main channel wall y_o.

PID	y_p (μm)	$v_{initial}$ (m/s)	$Re_{expected}$	$Re_{experimental}$	Output
1	7.5	6×10^{-4}	0.008	0.0005	Main
2	8.1	0.002	0.008	0.0005	Branch
3	8.1	6×10^{-4}	0.008	0.0005	Branch
4	7.7	0.002	0.008	0.0005	Branch
5	7.6	0.021	0.08	0.003	Branch
6	11.6	0.01	0.08	0.003	Main
7	7.7	0.02	0.08	0.004	Branch
8	7.7	0.02	0.08	0.004	Branch
9	7.5	0.019	0.08	0.007	Branch
10	8.2	0.012	0.08	0.007	Branch
11	12.1	0.008	0.08	0.007	Main
12	16	0.105	0.8	0.02	Main
13	17.5	0.124	0.8	0.02	Main
14	12	0.144	0.5	0.03	Main
15	13.5	0.112	0.5	0.03	Main
16	13.3	0.155	0.8	0.04	Main
17	16	0.193	0.8	0.04	Main
18	13.5	0.163	0.8	0.04	Main

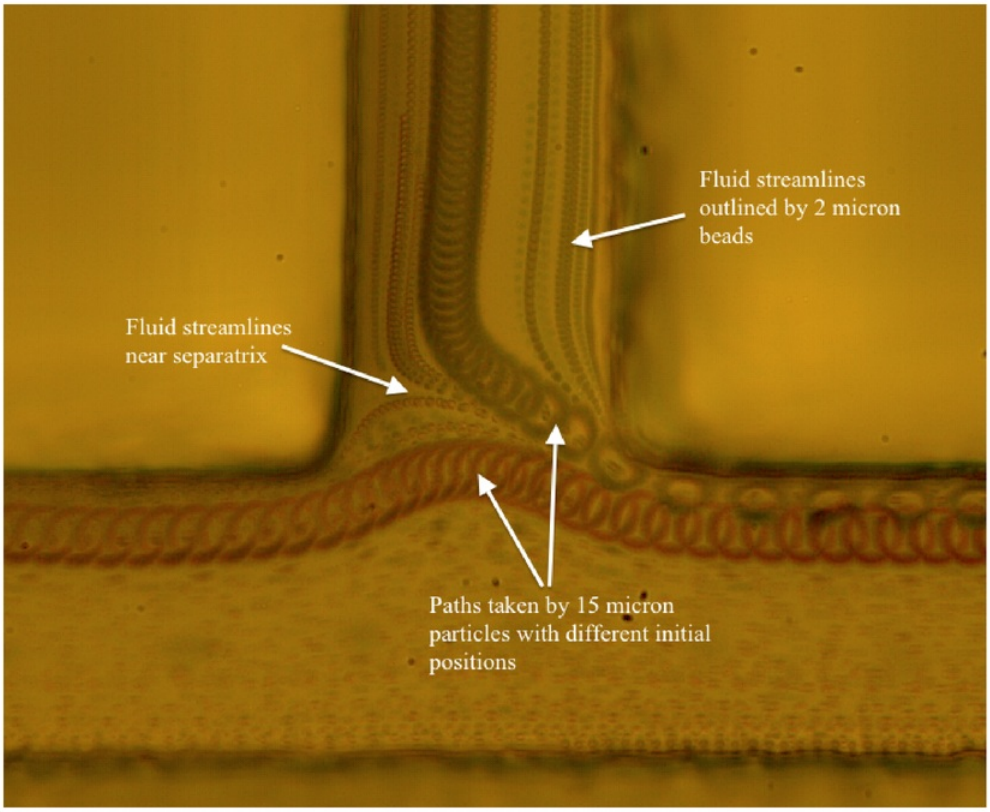

Figure 4.4: Video projection of points in Fig.4.1 that the particles pass through in the channel bifurcation. The particles paths that the points collate to clarify the particle pathways and help determine motion around and at the separatrix line.

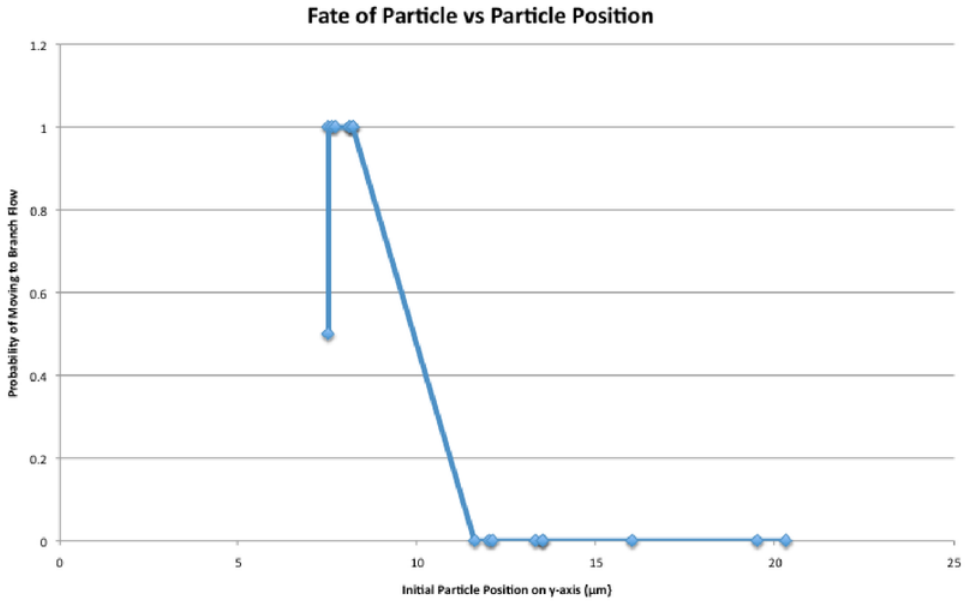

Figure 4.5: Graph showing the probability of the particle moving up the branch flow for various initial particle positions (y_p).

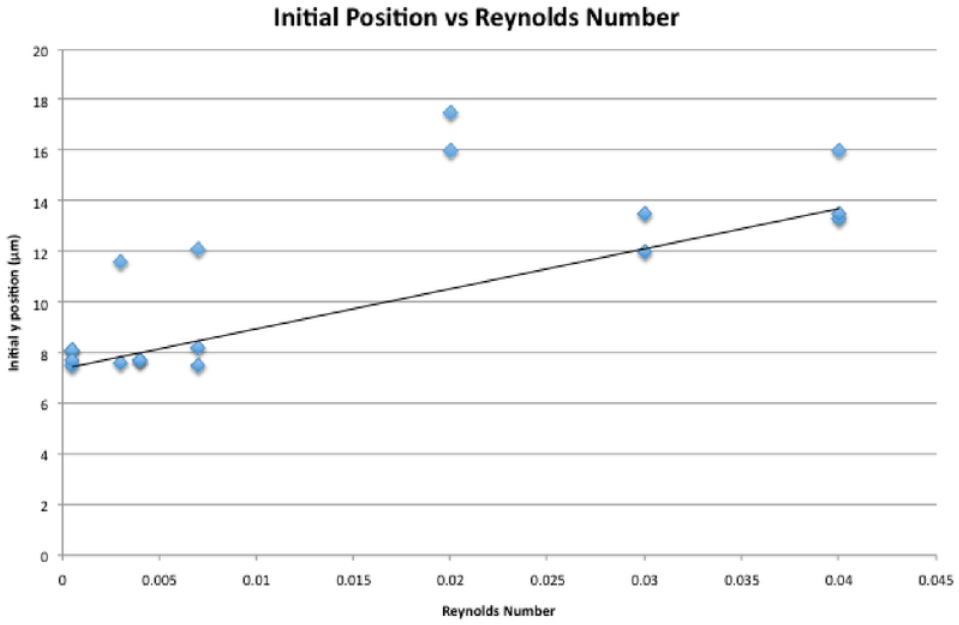

Figure 4.6: Graph showing the increase of the initial position seen with Reynolds number. A trendline was place the minimum values across the data to show this relationship.

Chapter 5

Discussion

5.1 Particle Fate with Increasing Reynolds Numbers

The major component of this work is determining the how larger particles interact with fluid flows at different Reynolds numbers. Although the sample size of the data extracted from videos taken from the experiment was sub-optimal it has unveiled details about the processes and given some direction to the future analysis in faster microfluidic continuous flow procedures.

From the results that has been gathered from the data suggests that their is some correlation between the fate of the particle, Reynolds number and the initial position of the particle moving in the flow. Doyeux explains this correlation using a bifurcation geometry that have symmetrical output branches that are perpendicular the input flow that can be varies so that the flow rate in one branch is higher than the other. That explanation can also be used for the movement of particles in the geometries of this experiment. Fig.5.3 and Fig.5.2 show the pressure differentials between the particle and the wall for asymmetrical bifurcation outputs, the low flow rate branch, Q_1 and high flow rate branch (main flow), Q_2 as the particle approaches the bifurcation and at the stagnation point between the flows. The results from the particle tracking of 15 μm spheres as the particle approaches the bifurcation has shown different behaviours as Reynolds numbers were increased. The initial tests at lower Reynolds numbers, between 0.5×10^{-4} to 0.4, shows the focusing of particles onto wall leaves little or no gap between the particle surface and the wall for most of the particles studied, these particles therefore had an initial position of approximately 7.5 μm. This follows the expected theoretical result for low Reynolds number in Fig.5.3 and should be reinforced by the initial attraction to the low flow rate branch which affects the initial distribution of the particles [15].

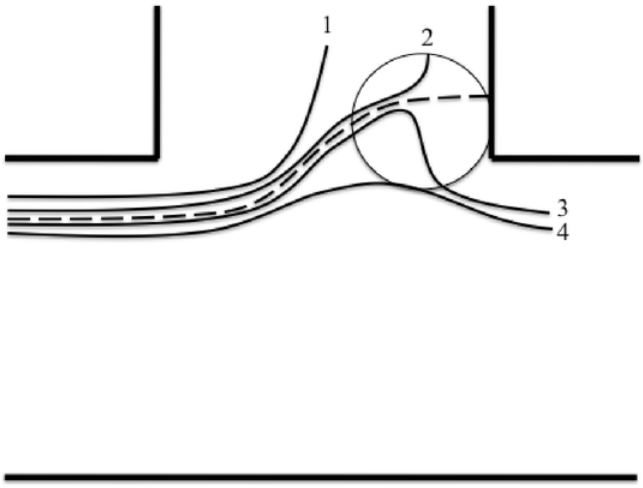

Figure 5.1: This figure show the different kinds of paths particles took depending mostly of there initial position on the y axis. Particles at low Reynolds numbers had trajectories of usually 1 or 2. Particle at higher Reynolds number of 3 or 4. The dotted line show the fluid separatrix where the behaviours change, particles with initial positions above the separatrix would follow 1 or 2 whilst those below 3 or 4.

In the results observed below Reynolds numbers of 3×10^{-4} the behaviour of the particles with initial positions near the separatrix line favoured the low flow rate branch however the probability of the particles moving into high flow rate branch shown in Fig.4.5 shows that the large particles do not always favour the low flow rate branch. This was interesting as the fluid separating lines shown by the 2 μm particles near the separatrix appears to lie beneath the centreline path of the particle like in Doyeux et. al results. So due to Reynolds number causing very slow creeping flows these particles may have cross streamlines back into the high flow rate flow as it seems harder to overcome the original pressure difference or otherwise the resistance of the P'_2 may have increased causing the particle to be attract towards the. This type of motion occurred when the particle path was near the separating line otherwise particles moved into the branch flow.15 μm Particles that reached the bifurcation at flows with Reynolds numbers between 3×10^{-4} to 7×10^{-3} had most of the particles had move to the low flow rate output branch. In these flows particles would separate distinctly based in the original position in relation to the separatrix line. Particles above the separatrix would move to the Q_1 and those below to Q_2. As particles were placed close to the wall of the channel the particles preference was mainly towards Q_1 including when particles closely followed the separatrix.

As we increased the flow rates to achieve higher Reynolds numbers of 0.02 to 0.04 the particles observed start to be elevated off the wall even though they were being

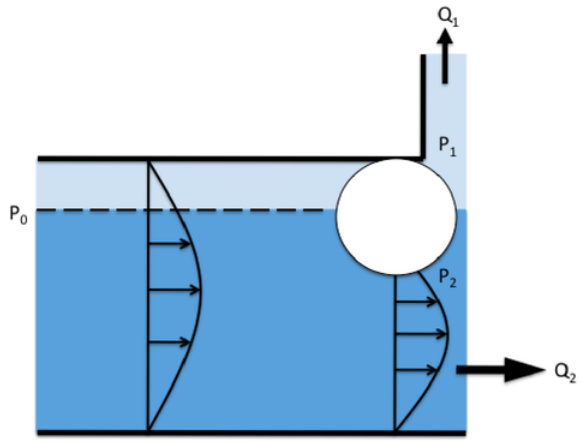

Figure 5.2: This figure offers a simplified look the pressures difference around the rigid particles before reach the bifurcation. Where there is a theoretical attraction to low flow rate branch if particles are situated near the channel wall. Q_1 is the branch flow and Q_2 is the main flow.

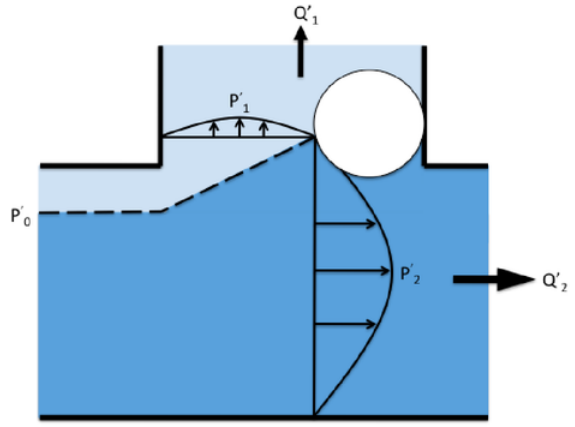

Figure 5.3: This figure offers a simplified look the pressures difference around the particles as it reaches the stagnation point where separatrix lies. This shows how the asymmetrical flow of a perpendicular channel separates the pressure regions across its geometry. The particles here should have an attraction to the high flow rate branch as now $P_1' > P_2'$. Q'$_1$ is the branch flow and Q'$_2$ is the main flow.

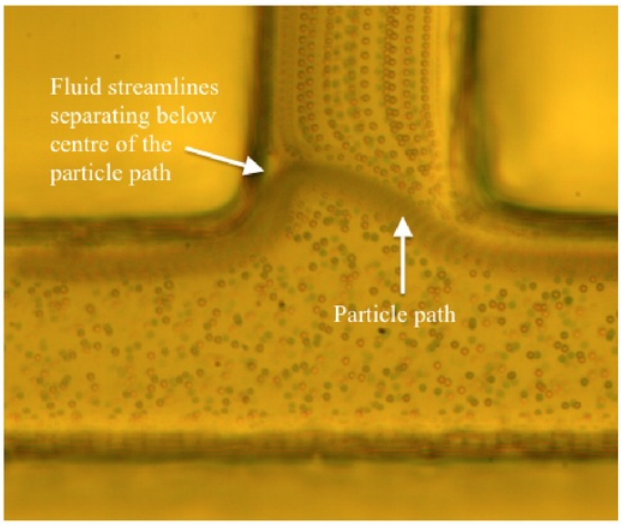

Figure 5.4: This figure show the video projection of the particle path taken by a 15 μm particle at Re = 0.0005 crossing the fluid separatrix to move into the high flow rate channel.

focused using the buffer solution. All the particles observed at this speed move into Q_2. The effects of pressure difference here have changed slightly as most particles are away from the wall the difference between the pressures changes so that P_1 increases and P_2 decreases. Then as P_1 change to P'_1 the pressure drop not as effective as the centre of the particle now lies below P'_0 where the pressure profile of Q_2 below the particle is now lower. The question at these higher Reynolds number is to why the directing of particles close to the wall for higher Reynolds numbers failed to keep the particles near the separatrix, causing them to follow streamlines leading into the main channel flow and how mitigate them? The cause of this movement away from the channel wall may be due to the inertial lift experienced by the particles as particle Reynolds number increases with shear stresses of the fluid velocities around it. This effect may be minor at Reynolds numbers but it is still enough to throw the particles 3 μm off the wall which is enough to move it off the separatrix line, at least for this system. The effects of inertial lift has been described using the particle Reynolds number, R_p, the expresses the inertial and viscous forces acting on the particle. This particle Reynolds number changes almost solely dependant on the radius, a. Di Carlo explored this in his paper relating the radius to the lift force from the shear lift, F_s, from the velocity change and the wall force, F_s, where $F_s \propto a^2$ and $F_w \propto a^3/\delta$ where δ is distance from the wall. In the experiment we primarily used 15 μm so if we keep the a constant then the force is proportional to the distance from the wall. As the particles are focused on the wall it would not be unreasonable to say that the particles could be shifted away from the wall by these lift forces. The graph in Fig.4.6

shows this movement away from the wall as Reynolds numbers increased. The equation for net lift Equation 2.13 is proportional to the the flow Reynolds numbers so what needs to be quantified is how the distance, δ changes as Reynolds number increases. It appears that the relationship between the Reynolds number and initial position increases linearly once the lift force surpasses the drag forces on the particle. More points between those Reynolds numbers need to studied before any conclusions can be made however modelling this behaviour can give insight.

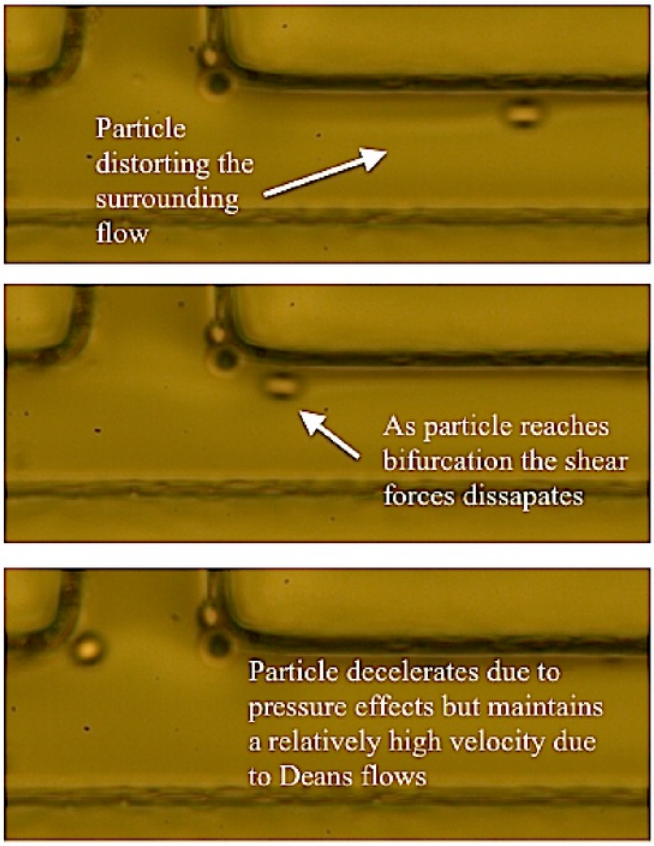

Figure 5.5: This figure shows a 15 μm particle travelling through the device at a Reynolds number of 0.02 with no 2μm particles. As the particle moves through the channel the Deans flow around the particle acts to push the particle from the wall and create a flow that pushes particles from the low flow rate branch.

The other interesting effect that occurs at high Reynolds numbers in how the

shear forces act on the particle as they cross the bifurcation. In some of the experiments at high Reynolds numbers the refraction of light on fluid flows highlighted these effects as seen in Fig.5.5. The particles due to the shear forces on it act to lift the particle from the wall and also distorts the flow around it, the particle maintain quite a fair distance with an initial y position of 13 μm from the wall so the wall effect seems to also occur. When the particle reaches the bifurcation the pressure effects of Fig.5.2 then act on the particle as talked about before that leads the particles moving into the the main flow streamline. The initial effects add to this as the shear force from the flows transfers across the particle to pull the particle forward as the pressure that was P_1 in Fig.5.3 now acts in the opposite direction, so the particle doesn't experience the same change in pressure as in the low Reynolds numbers case. However the shear lift effect is a residual acting component of the particle path due to Deans flows. This effect should also be explored deeper for a better understanding of high Reynolds number flows.

5.2 Bifurcation Geometry Separatrix

In this experiment it appeared that the fluid separating line did not strongly differentiate from the centreline of the 15 μm. Doyeux et. al said that for the attraction towards the low flow rate branch that acts before the particle moves back along the high flow rate branch is due to the relationship between the initial position of the fluid separating line. The T-shaped bifurcation geometry he used was symmetrical output where this experiment the outputs were asymmetrical. The major difference between the trajectories found in this experiment and Doyeux et. al is that the separatrix line was very similar to the centreline of the large particles in our experiment whereas he found the separatrix to lie above the centreline of the particle before the particles would cross the streamline into the low flow rate branch. The point of which the particles that I found where the particles would cross streamlines in for very low Reynolds number flows otherwise the direction of particles were more dependant on whether the centreline of the particle was above or below the separatrix. To observe cross streamline behaviour seen in Doyeux it may be necessary to expand the channel length to observe trajectories past the 50 μm channel. It does not seem like these geometries will be useful for attracting large particles down low the flow rate branch and a change in approach will be required if large particles are to be drawn to the low flow rate with inertial effects considered.

Chapter 6

Conclusion

This paper manages to show some insight into how moderate Reynolds number flows affect the separation of particles. At low Reynolds numbers particles with initial positions close to the wall are attracted mainly to low flow rate branch for the exception of some at very low Reynolds numbers, this behaviour needs to be tested with more particles to confirm a change in these flows. At higher Reynolds numbers particles are observed to move away from the wall due to the shear forces on the particle that occur as the inertial forces begin to get larger than the viscous forces. A number of microfluidic effects cause the particles to show different behaviours to the low Reynolds number flow rate. These effects need to be further studied in order to define particle movement at these higher Reynolds number as well be matched with more extensive data in the future.

Chapter 7

Future Work

7.1 Improving Experimental Results

7.1.1 Visualisation of Channels

When observing channels through an inverted microscope the image can be distorted by how the light interacts with the surface of a LOC device. The walls of the device blur the more the camera focuses on a one particular layer over a layered 3D surface due to the bending of light into the camera lens. This ends up sometimes making it difficult to pin point the location of particles relative to the channel surfaces. A way to combat these visual problems is adjusting index refraction parameters. By using liquids with same refractive index as the channels the visibility of the channel and edges can be improved. This may be considered for future tests in PDMS devices under microscopes.

The secondary visualisation challenge was to capture particles that were travelling at higher speeds, taking into account that even at the fastest camera frame rate the high speed camera can only take approximately 10 images for Reynolds numbers of 0.1, the exposure time should be increased in order to at least see the particle paths from high speed videos captured at these speeds.

7.1.2 Losses in Channel Flows

One notable occurrence that has been marked down on the table is the change from the expected Reynolds number to the experimental value found by measuring small particles along the main channel like track 4 from Fig.4.1. Losses of approximately 90% in Reynolds number values which mostly comes from flow rate changes in the channels and difference

pressure between the inputs and outputs. The experimental setup allowed for the reservoir exiting the outputs to be sent to a reservoir that was place level or at slightly elevated positions when compared to the height of the syringes, this may have created a back pressure causing the flows to slow down relative to this pressure. The secondary reason why the flow rate may have changed is because of the pressure near the ports causing the liquid to leak from the chip this was noticed when running the device and can be seen in the image of the device in Fig.7.1. The main leakage came from the higher flow rate inputs from the 10mL syringe suggesting that the PDMS did not withstand the pressure at those points. If testing of LOC device at Reynolds numbers around 1 or may it caution in device fabrication may be needed or rethought to ensure no leakages for future device fabrication. A solution to these leakage problems might be to simple change the luer ports to an input system that takes smaller more flexible tubing to ensure that the fluids are injected into the device instead of building up pressure around it.

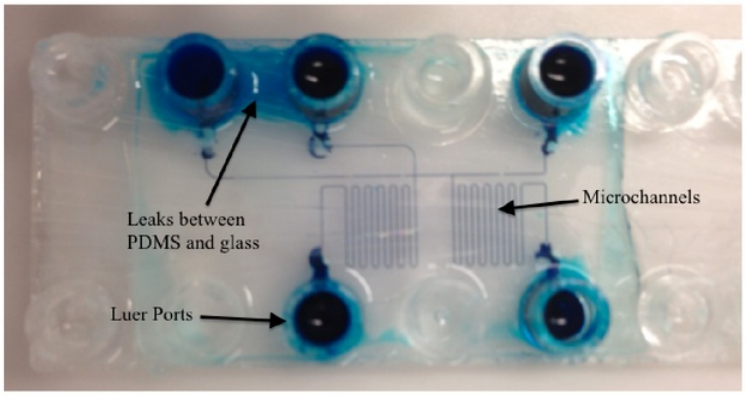

Figure 7.1: Device flooded with blue ink showing parts of the device and where leaks would occur.

7.2 High Throughput Filtration

The aim of this experiment is to determine ways to achieve a high throughput of particles at bifurcations for the purposes of separating solution such as blood for clinical usage and diagnosis. If larger particles are to move into the low flow rate branch modification to the channel geometry will need to be done to manipulate the pressure differentials around the particles to favour the low flow rate branch. One idea would be to add a slope to the bottom of the bifurcation constricting the main flow this should theoretically cause the particle to want to move to the low flow rate branch. To observe the low Reynolds number observations in Doyeux et. al work the channels can be expanded to better observe the trajectory of particles in the flow as well.

If this experiment is run again with the same parameters I would suggest controlling the inputs and outputs using pressure controlled pumps. This should allow for much more reliable results and a high throughput of large particles as particle often get clogged around the inputs.

Chapter 8

Abbreviations

LOC	Lab on chip
PDMS	Polydimethyl siloxane

Appendix A

Equations

$$p(dv/dt + (v.\nabla)v) = -\nabla\rho + n\nabla^2 v + f \tag{A.1}$$

$$F_{inertial} = \frac{\rho V^2}{L} \tag{A.2}$$

$$F_{viscous} = \frac{\mu V}{L^2} \tag{A.3}$$

$$\frac{F_{inertial}}{F_{viscous}} = \frac{\rho V L}{\mu} = Re \tag{A.4}$$

$$R_p = Re\frac{a}{L^2} = \frac{\rho V a^2}{\mu L} \tag{A.5}$$

$$\Delta p = R_{hyd} Q \tag{A.6}$$

$$v_x(y,z) = \frac{4h^2\Delta p}{\pi^3 \eta L} \sum_{n,odd}^{\infty} \left[1 - \frac{cosh(n\pi\frac{y}{h})}{cosh(n\pi\frac{w}{2h})}\right] sin\left(n\pi\frac{z}{h}\right) \tag{A.7}$$

$$R_{hyd} = \left(\frac{h^3 w}{12\eta L}\left[1 - \sum_{n,odd}^{\infty} \frac{1}{n^5}\frac{192}{\pi^5}\frac{h}{w} tan\left(n\pi\frac{w}{2h}\right)\right]\right)^{-1} \tag{A.8}$$

$$R_{hyd(rect)} = \frac{12\mu L}{1 - 0.63(h/w)} \frac{1}{h^3 w} \tag{A.9}$$

$$F_{drag} = -6\pi\mu a(v - u) \tag{A.10}$$

$$F_w = C_L \rho U_{max}^2 a^6 / D_h \tag{A.11}$$

$$F_L = C_L \rho U_{max}^2 a^3 / D_h \tag{A.12}$$

$$F_L = C_L G^2 \rho a^4 \tag{A.13}$$

$$Q = VA \tag{A.14}$$

Appendix B

Equipment

B.1 Overview

Here is the list of equipment used in this experiment.

B.2 Hardware/ Software

- Phantom high speed camera/software: high speed imagery.
- Inverted microscope/camera/NIS Elements: testing camera on inverted microscope in black and white.
- Colour microscope/camera/Toupview software: for taking stills of device.

B.3 Laboratory Setup

- Syringe pump: for moderating syringe speed.
- Syringes/ luer tubing.
- PPE: gloves, safety glasses.
- 15.5 micron microspheres (normal particles) Bangs Laboratories
- 10 micron microspheres
- 0.5 micron Bang Laboratories Polystyrene Dragon Green Microspheres.

- 2 micron Polychromatic Red Microspheres.
- Glucose
- Pipette
- Distilled Water
- Cleaning products. MA 0.01 Alkaline and 2-Propanol

Bibliography

[1] D. Mark, S. Haeberle, G. Roth, F. von Stetten and R. Zengerle, "Microfluidic lab-on-a-chip platforms: requirements, characteristics and applications", *Chemical Society Reviews*, vol. 39, no. 3, p. 1153, 2010.

[2] "Microfluidics in commercial applications; an industry perspective", *Lab on a Chip*, vol. 6, no. 9, p. 1118, 2006.

[3] L. Volpatti and A. Yetisen, "Commercialization of microfluidic devices", *Trends in Biotechnology*, vol. 32, no. 7, pp. 347-350, 2014.

[4] C. Shields, K. Ohiri, L. Szott and G. Lpez, "Translating microfluidics: Cell separation technologies and their barriers to commercialization", *Cytometry Part B: Clinical Cytometry*, vol. 92, no. 2, pp. 115-125, 2016.

[5] N. Pamme, "Continuous flow separations in microfluidic devices", *Lab on a Chip*, vol. 7, no. 12, p. 1644, 2007.

[6] E. Sackmann, A. Fulton and D. Beebe, "The present and future role of microfluidics in biomedical research", *Nature*, vol. 507, no. 7491, pp. 181-189, 2014.

[7] Grossmann, V., Roller, A., Klein, H.U. et al. "Robustness of amplicon deep sequencing underlines its utility in clinical applications" *Journal of Molecular Diagnostics* pp. 473?84, 2017.

[8] Cinpolat, O., Unal, Z.N., Ismi, O., Gorur, A., Unal, M. "Comparison of microRNA profiles between benign and malignant salivary gland tumors in tissue, blood and saliva samples: a prospective, case-control study" *Brazilian Journal of Otorhinolaryngology* pp. 276?84 2017.

[9] H. Becker, *Lab Chip*, vol. 9, pp. 2759?2762, 2009.

[10] H. Bruus, *Theoretical microfluidics*, 1st ed. Oxford: Oxford Univ. Press, 2011.

[11] J. Beech, *Microfluidics Separationand Analysis of Biological Particles*,

[12] D. Di Carlo, "Inertial microfluidics", *Lab on a Chip*, vol. 9, no. 21, p. 3038, 2009.

[13] A. Bhagat, S. Kuntaegowdanahalli and I. Papautsky, "Inertial microfluidics for continuous particle filtration and extraction", *Microfluidics and Nanofluidics*, vol. 7, no. 2, pp. 217-226, 2008.

[14] B. Roberts and W. Olbricht, "Flow-induced particulate separations", *AIChE Journal*, vol. 49, no. 11, pp. 2842-2849, 2003.

[15] V. Doyeux, T. Podgorski, S. Peponas, M. Ismail and G. Coupier, "Spheres in the vicinity of a bifurcation: elucidating the Zweifach Fung effect", *Journal of Fluid Mechanics*, vol. 674, pp. 359-388, 2011.

[16] D. Inglis and N. Herman, "A scalable approach for high throughput branch flow filtration", *Lab on a Chip*, vol. 13, no. 9, p. 1724, 2013.

[17] M. Yamada and M. Seki, "Hydrodynamic filtration for on-chip particle concentration and classification utilizing microfluidics", *Lab on a Chip*, vol. 5, no. 11, p. 1233, 2005.

[18] E. Asmolov, "The inertial lift on a spherical particle in a plane Poiseuille flow at large channel Reynolds number", Journal of Fluid Mechanics, vol. 381, pp. 63-87, 1999.

[19] M. Yamada and M. Seki, "Microfluidic Particle Sorter Employing Flow Splitting and Recombining", *Analytical Chemistry*, vol. 78, no. 4, pp. 1357-1362, 2006.

[20] E. Sollier, M. Cubizolles, Y. Fouillet and J. Achard, "Fast and continuous plasma extraction from whole human blood based on expanding cell-free layer devices", *Biomedical Microdevices*, vol. 12, no. 3, pp. 485-497, 2010.

[21] Z. Wu, B. Willing, J. Bjerketorp, J. Jansson and K. Hjort, "Soft inertial microfluidics for high throughput separation of bacteria from human blood cells", *Lab on a Chip*, vol. 9, no. 9, p. 1193, 2009.

[22] Zhou and I. Papautsky, "Fundamentals of inertial focusing in microchannels", *Lab on a Chip*, vol. 13, no. 6, p. 1121, 2013.

[23] , T. Fujii, "PDMS-based microfluidic devices for biomedical applications", *Microelectronic Engineering*, vol. 61, pp. 907-914, 2002.

[24] D. Inglis, "A method for reducing pressure-induced deformation in silicone microfluidics", *Biomicrofluidics*, vol. 4, no. 2, p. 026504, 2010.

[25] J. Martel and M. Toner, "Inertial Focusing in Microfluidics", *Annual Review of Biomedical Engineering*, vol. 16, no. 1, pp. 371-396, 2014.

[26] "Fluidigm — Products", Fluidigm.com, 2017. [Online]. Available: https://www.fluidigm.com/products. [Accessed: 03- Nov- 2017].

[27] "i-STAT System — Abbott Point of Care", *Pointofcare.abbott*, 2017. [Online]. Available: https://www.pointofcare.abbott/int/en/offerings/istat. [Accessed: 03- Nov- 2017].

[28] "BMC - Experimental Procedures — Advanced Lab", *Experimentationlab.berkeley.edu*, 2017. [Online]. Available: http://experimentationlab.berkeley.edu/node/84Viewing.2FTrackingParticlesinViscousSuspen [Accessed: 05- Nov- 2017]

[29] "Phantom High Speed Cameras — Super Slow Motion Cameras", *Phantomhighspeed.com*, 2017. [Online]. Available: http://www.phantomhighspeed.com/Products/PhantomCameraProducts. [Accessed: 05- Nov- 2017].